Engineering Structures 294 (2023) 116749

Contents lists available at ScienceDirect

Engineering Structures

journal homepage: www.elsevier.com/locate/engstruct

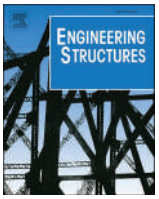

Shear strength of the anchor embedded into masonry

Paolo Foraboschi

Università IUAV di Venezia – Dipartimento Culture del Progetto, Dorsoduro 2206, 30123 Venice, Italy

ARTICLE INFO

Keywords:
Adhesive anchor
Floor masonry connections
Joist masonry connections
Masonry anchor
Masonry attachment connections
Mechanical expansion anchor
Metal injection anchor
Shear anchor
Straight shaft anchor

ABSTRACT

This paper focuses on any straight bar, herein called "anchor", inserted within a hole drilled into a masonry structure, installed orthogonally to the masonry surface, and bonded to the masonry either with an anchoring material or without (adhesive or mechanical anchors). The anchor is subjected to a transverse force applied at the end that protrudes from the masonry (i.e., a shear force having direction parallel to the masonry surface), while no appreciable axial force is applied to the anchor (shear anchor). In brief, the paper is devoted to the post-installed horizontal anchor that transfers vertical loads from a horizontal structure to a vertical masonry structure.

On site experiments on real anchors allowed the author to establish the mechanical assumptions that govern the behavior of the shear anchor. Based on those assumptions, an analytical (closed form) model was created. The model is comprised of a function that gives the ultimate contact pressures, and a two-equation system whose solution is the maximum shear force that the anchor can bear, therefore called "shear strength". The model also provides the elastic limit shear strength. The data to be entered into the model is composed of the geometry of the anchor and the strength of the masonry.

The paper presents the experimental campaigns, the model, the application of the model to case studies, and a comprehensive discussion. The results put forward the optimal technical solutions for the masonry shear anchor, which are described.

1. Introduction: framework, subject matter, study's statement of purpose, background information

This paper, which aims to fill a gap in scientific and technical literature about anchors, provides an analytical, closed form mathematical model that predicts the shear strength of an anchor embedded into a masonry structure.

Remodeling, restoring, rehabilitating, and upgrading existing masonry buildings often require connecting new horizontal structures to existing masonry structures, or to strengthen the existing connections.

More specifically, beams, girders, floors, plates, decks, joists, trusses, lintels, balcony, etc., made of reinforced concrete, steel or timber must be supported by masonry structures such as walls, perforated walls, panels, columns, vaults. If the horizontal structure cannot be rested on the top horizontal edge or on a taper of the masonry structure, or otherwise cannot be inserted into the masonry (by a perforation), it must be mechanically fastened to the masonry structure. It should be noted that large perforations are often forbidden in historical buildings.

Fastening must be accomplished by inserting one or more connecting elements into the already built masonry structure. That connector is here called "anchor" and a connection with more anchors is called "anchor group". The typical fastening solution to connect the horizontal structure to the existing masonry vertical structure is a horizontal anchor post-installed into the masonry [1–3].

That anchor, which is called "shear anchor", is the topic of this paper. More specifically, the present paper focuses on the single shear anchor or on the shear anchor of a group in which the shear strength of an anchor does not depend on anchor spacing, so that the shear strength of the group is equal to the sum of the shear strengths of each individual anchor.

The structural assembly external to the surface of the masonry, which transmits loads to (or receives loads from) the anchor, plays no role in the strength and performance of the anchor that this paper focuses on. For the sake of simplicity in exposition, it is hereinafter called "attachment".

For the sake of avoiding useless multiplicity of terms, the masonry structure that is herein considered is the wall. It being understood that this paper includes all types of masonry structures.

One end of the anchor is embedded into the masonry (internal end) and the other end (external end) may be collected by a bearing steel

E-mail address: paofor@iuav.it.

https://doi.org/10.1016/j.engstruct.2023.116749
Received 22 May 2023; Received in revised form 18 July 2023; Accepted 7 August 2023
Available online 15 August 2023

plate, which is a component of the attachment. The external end of the anchor passes through a hole of that steel plate. That hole is usually unthreaded but could be threaded. The anchor can be joined to the steel plate by a nut (or a locknut, or else together with a locknut), a weld, or using headed anchors (conventional hex-head, square head threaded screws, which however are less customary, or hexagonal socket screws, etc.), or else using a countersunk screw anchor (which does not protrude from the steel plate). Otherwise, the external end may be embedded into the concrete or timber composing the attachment.

The steel plate, which is placed on the masonry surface, restraints the rotation of the segment that protrudes from the masonry. The steel plate supplies therefore the anchor with supplementary shear strength. Likewise, the embedment of the external end into concrete or timber provides the anchor with supplementary shear strength, owing to some dowel action. Considering that typically those extra strengths are no more than moderate (as proven by these experiments), they are here neglected. Accordingly, the way the anchor is joined to the attachment plays no role in the shear strength. The external end of the anchor is hence modeled as free, which is a simplifying and conservative assumption.

This paper uses the term "block" to refer to the masonry unit and the term "joint" to refer to the mortar bond.

This paper considers: both older and modern masonry; blocks made of bricks, stones, or concrete (brickwork, stonework, concrete work); all types of bricks (handmade or industrial bricks); all types of stones (wrought and arranged in any fashion); joints made of lime mortar (hydraulic, non-hydraulic, or semi-hydraulic lime), lime-cement mortar, or cement mortar.

1.1. Topic of the research work

This paper is concerned with an anchor inserted into a masonry structure, used to transmit applied loads that induce a force transverse to the anchor, applied at the end of the anchor that protrudes from the masonry surface (Fig. 1). That force is here called "shear force" and is denoted by V. The ultimate value of the shear force, which is the shear strength of the anchor, is denoted by V_u. The paper presents an analytical model to predict V_u.

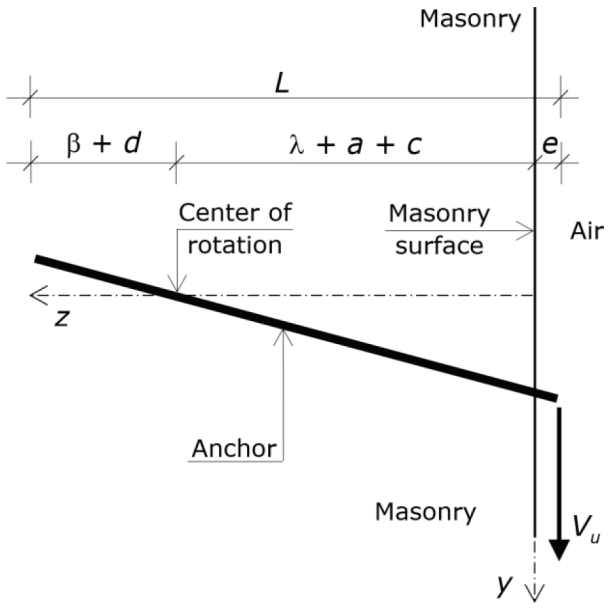

Fig. 1. Reference structure: Anchor, semi-space whose surface separates the masonry from the air, ultimate shear force, axes y and z, other symbols. Failure mode: Rotational mechanism. In real anchors the force is directed downwards, while in the experiments the force was directed upwards. The maximum shear may bend the length that protrudes from the masonry surface.

The collocation "shear force" refers to the orthogonality of the external force V to the anchor, being the former vertical and the latter horizontal, while the internal forces in the anchor due to V are both shear force and bending moment (no axial force).

1.2. Single anchor and anchor group

The single anchor can behave dramatically different than the anchor that is part of a group. The first difference is that a close spacing generates the anchor group effect, which causes the shear strength of the anchor group to be lower than the sum of the shear strengths of each anchor as single (individual) element [4–8]. However, this difference exists only in the case of close spacing, which is not considered herein. But there is another difference, which is significant and can never be eliminated; it can only be mitigated.

The force V is, more or less, always eccentric to the masonry surface and that eccentricity induces a couple in the anchor, which is equal to the shear force multiplied by the eccentricity (Fig. 2).

Moreover, even if the connection of the attachment to the anchor is a hinge, it ever transmits a certain couple, since it cannot be a pure pin. Whereas if it is fixed, the couple is substantial. Thus, the connection induces another couple, which adds to the previous one.

Ultimately, any connection implies not only a shear force but also a resulting moment acting on the anchor/anchors, which is the sum of a couple due to the eccentricity of the shear force plus a couple due to the actual rotational behavior of the connection.

In the case of a single anchor this moment acts on the segment that protrudes from the masonry. The resisting mechanism against this moment is the same as against the shear force, which consists of transverse contact pressures that equilibrate the shear force (Figs. 2 and 3). On one hand, this model accounts for this moment, given that it does not modify the behavior of the anchor. On the other hand, however, this moment reduces the strength of the anchor, since it exploits some fraction of the shear capacity, and therefore must be kept as small as possible [7,9,10].

In the case of an anchor group this moment acts on the whole group. The resisting mechanism against this moment is different than that against the shear force; the latter consists of transverse contact pressures while the former of both a longitudinal compressive force and a longitudinal tensile force equal and opposite acting on the whole group (i.e., the former is represented by a bending couple acting on the entire group). The compressive force induces contact compressive stresses on the masonry surface, which play no role in the shear strength. Conversely, the tensile force introduces tensile axial forces in some anchors of the group, which modify the behavior and performance of these anchors [11–14]. In fact, the resisting mechanism against axial force consists of longitudinal tangential stresses that equilibrate the axial force [1,2,15]. The strength of that mechanism is dictated by the masonry extraction force (pull-out resistance of the anchor). The prediction of the extraction force requires a specific model, which can be borrowed from the literature [16–21]. However, the result of such a model (axial anchor) cannot be superimposed to the result of this model (shear anchor) because of the substantial interaction between shear and axial behavior, which requires accounting for the combined effect.

Nevertheless, the real point is not that this model does not cover the combined effect of shear force and axial force, but that the interaction impacts dramatically on the resisting capacity, which implies that the axial force drastically reduces the shear strength of the anchor.

Therefore, the design of an anchor group should cut down the moment (the bending couple) that acts on the anchor group as much as possible, so as to introduce no more than marginal axial force in the anchors. Accordingly, in order to be properly designed, an anchor group needs that the eccentricity be the smallest possible and that the connection between attachment and anchor group be a hinge with no more than small imperfections (never a fixed connection).

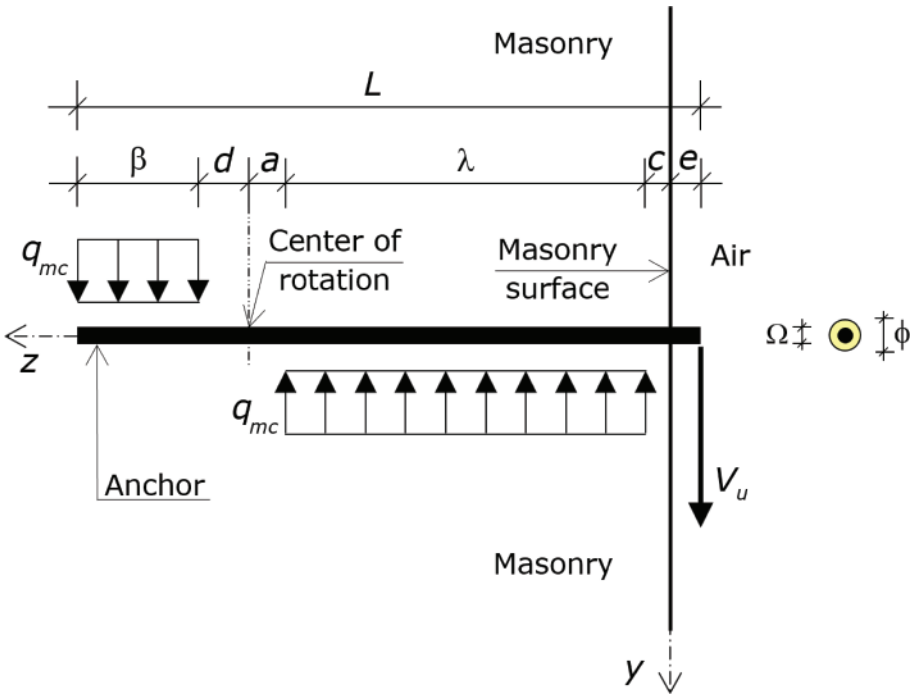

Fig. 2. Contact pressures q_{mc} acting onto the anchor at failure, including the relevant symbols. The pressures q_{mc} are uniform not only along the anchor's length, as shown by the figure, but also along the anchor's width (Fig. 3). The magnitude of the load acting per unit length of anchor is hence $\phi \cdot q_{mc}$. The same pressures with opposite direction act on the drilled hole. The cross-section on the right refers to the adhesive anchor. In the case of mechanical anchor, $\Omega = \phi$.

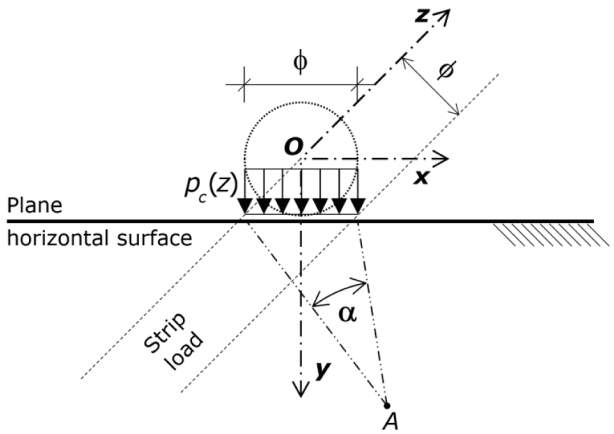

Fig. 3. Semi-space whose surface lies on the x-z plane, at $y = \phi/2$. Generic contact pressures p_c acting uniformly over the masonry at a certain abscissa z (the contact pressures p_c at failure are denoted by q_{mc}). Cartesian coordinate system, whose origin is at the center of the anchor, and α-coordinate system, with reference to the pole A.

Likewise, an anchor whose axis is not orthogonal to the external force suffers from the combined effect of shear and axial forces, so it should not be designed and built.

To sum up, the anchor this paper focuses on is either single or part of a group whose group effect and global moment are negligible.

1.3. Adhesive and mechanical post-installed anchors

Typically, the anchor is made of metal, in general steel (carbon, zinc-plated carbon, stainless, galvanized, or titanium steel). Nevertheless, it can be made of Fiber-Reinforced-Polymers, as long as the strength hierarchy specified in Subsection 1.4 is fulfilled.

The anchor can be a bar, a bolt, a nail, a screw, a rod, a stud, a pin, a sleeve, a wedge shank, an expansion bolt, a wedge expansion bolt, a split drive shaft, a strike shaft, a drop-in shaft, a self-drilling screw, a lag shield screw. In short, the anchor that this paper refers to is any straight hot-rolled or cold-rolled piece of metal embedded into masonry [22,23].

That variety of anchors can be grouped into two main categories (Fig. 2) – namely, adhesive and mechanical [24,25]. In turn, mechanical anchors can be divided into two sub-categories – namely, screw-type and wedge-type anchors [24,26]. The choice on which type of anchor to use depends on the project at hand. Accordingly, installation of anchors can be done in two ways – namely, chemical or mechanical.

An adhesive anchor achieves resistance by bonding with adhesive [3,25–34]. Chemical post-installation requires drilling a hole into the masonry, filling the hole with an anchoring material, and inserting the anchor into the drilled hole, which implies the anchoring material in excess be expelled outside or penetrates the voids of the surrounding masonry (excess adhesive must be removed from the masonry surface). Post-installation is completed when the anchor touches the bottom of the drilled hole. Adhesive anchors must be cured at adequate temperature and number of days before being loaded. As it cures, the adhesive forms a chemical bond between the masonry and the anchor. The anchor must be kept in the right position before the anchoring material has hardened.

The anchoring material can be based on resin or mortar (cement or hydraulic lime mortar). In the case of lime mortar joints, the only cement mortars that can be used are those based on pozzolana.

A mechanical anchor achieves resistance by taping its own hole as the screw is driven into the masonry, or else by means of expansion against the masonry or a sleeve [21,24,33–38]. Mechanical insertion into masonry of the screw-type often requires drilling a pilot hole. Then, threads on the anchor itself engage with the masonry that bounds the pilot hole to form a mechanical bond (or the threads engage with the hole directly formed by driving the anchor). Mechanical insertion of the wedge-type depends on a two-step process, besides drilling the hole. The anchor is driven into the drilled hole, then torqued down, causing an expansion of the mechanical anchor. That behavior exerts pressure against either the boundary of the hole or against a sleeve at the bottom of the hole to spread and grip the masonry, creating friction and holding

power. Mechanical anchors are designed to go into the hole in the base material but will not come out.

Not only does this paper include all the types of anchors, but also the model does not make any difference between the anchors, given that the way the anchor is installed impacts only on the extraction force but not on the shear strength. In the case of adhesive anchors, nevertheless, the way an anchor is installed impinges on the diameter of the drilled hole because the gap between anchor and drilled hole must be related to the anchoring material [21,24–27,29,32,33,36].

A resin is relatively soft. In order to prevent relative displacements of the anchor to the drilled hole, the layer of resin mustn't be thick. For resin anchoring material, thus, that gap should be no more than 1.5–3.0 mm for small diameters and no more than 4.0–7.5 mm for large diameters.

A mortar is sufficiently stiff to prevent the relative displacements of the anchor to the drilled hole while, in order to be correctly injected (homogeneously, without segregation or bleeding), requires that the gap be sufficiently large. For mortar anchoring material, thus, the gap should be no less than 3.5 mm for small diameters and by no less that 6.0–8.0 mm for large diameters.

Obviously, masonry allows only for post-installation. Hence, masonry cast-in anchor does not exist. In fact, a masonry cannot be built after the anchor has been previously placed, as it occurs for the concrete. The masonry anchor consists hence in a straight shaft, i.e., a shank without a hook at the embedded end. Moreover, no nuts, washers, or plates are attached to the embedded shaft.

The whole system – anchors, anchoring material, drilled hole, and masonry that surrounds the drilled holes – is here called "anchorage".

1.4. Strength hierarchy and specific requirements

The anchor that is considered here satisfies a strength hierarchy criterion according to which the shear strength is dictated by the masonry that surrounds the anchor.

The strength hierarchy implies that the metal of the anchor and the anchoring material must fail for shear forces V greater than the shear strength V_u. Accordingly, the metal and diameter of the anchor must be sufficiently capable of exploiting the entire capacity of the masonry, and the anchoring material mustn't be the weakest component of the anchorage. Those requirements are not modeling assumptions but basic construction rules.

The strength hierarchy also implies that the anchor has adequate clearance from the boundaries (edges) of the masonry wall and from the other anchors (if it belongs to a group), so that the shear strength V_u depends neither on the distance from the boundaries nor on the spacing of the anchors. According to [3,4,6,21–23,27,35], the former requirement is satisfied if the distance of the anchor from an edge parallel to the shear force is greater than 3.0 times the anchor's diameter, and the distance from an edge perpendicular to the shear force is both greater than 12 times the anchor's diameter and no less than 2.5 times the thickness of a block. The latter requirement is satisfied if the spacing of the anchors is greater than 2.5 times the anchor's diameter [5–8].

Ultimately, the anchor should be placed sufficiently far from the edges and the anchors must be adequate spaced, so as to develop the maximum potential shear strength.

Nevertheless, sometimes the specific design conditions do not allow such limits to the distances to be satisfied, which entails that the real shear strength is dictated by the edge effect or the anchor group effect [7,10,29,39–47], and hence it is lower than V_u predicted by this model. The satisfaction of the strength hierarchy shall be ascertained by a final verification that compares V_u to the strengths dictated by the other failure modes. The real anchor's shear strength will be the lowest one.

In addition, the strength hierarchy implies that V mustn't be resisted individually by a joint, but by the whole masonry. In fact, an anchor's shear strength dictated by the mortar would be no more than moderate, even slight in the case of historical masonry. Again, this is not a restriction of the model but a requirement for an anchor to be well-designed and properly installed [1,3,20–24,29,48–51].

A favorable exception, which can be accepted, is a shear strength dictated by the block instead of the whole masonry assembly. That exception can occur in the case of stonework with relatively large size stones (with the anchor inserted in the middle of a stone), while it cannot occur in the case of brickwork, as the brick's thickness cannot be sufficiently greater than the anchor's diameter.

Because they depend on a great variety of specific circumstances, the conditions that define whether anchor's shear strength is dictated by masonry strength or block strength are impossible to be generalized. So, the model presented here allows the user to choose which strength to utilize in each specific case, i.e., whether the masonry strength or the block strength. The case studies presented here have used masonry strength, which is the general and safe position.

In order to be skillfully executed the anchor must also be post-installed in a portion of masonry that is uncracked. However, this research has demonstrated that the uncracked portion can be relatively small (Section 7).

1.5. Prior-absent predictive mathematical tool provided by this research

Connections of structural members to masonry or concrete structures have been the subject matter of many valuable papers. Some of the mainstream papers about shear and axial anchors have been cited in the preceding subsections. Other milestone papers in the area of masonry shear anchors and allied areas are [52–61]. But those papers do not cover the subject matter of analytical prediction of the strength displayed by a post-installed anchor subjected to shear (transverse) force.

Regarding the shear strength of the anchor embedded into a masonry structure, the literature provides empirical [1,27,30,35,45,47–52,59–61] and numerical [28,29,31,32,35,36,38,55,58] methods, while the only analytical formulations that can be found [62,63] predict what in this paper is called "block surface failure" (subsection 5.3). However, block surface failure is one of the typical modes of collapse for cyclic loading, while for monotonic loading it is a local failure mode that occurs only seldom and never dictates the shear strength of the anchor. In fact, those formulations are devoted to seismic analysis (or to anchors close to the edges), while for static analysis the predictions of those formulas can only be used to define a free parameter of this model, i.e., the length c.

Masonry shear anchor is also included into codes, requirements, specifications, standards, provisions, edited by organizations for technical assessment [3,7,20–23,25,26,33,39–44,64–66]. But again, those documents do not include the analytical prediction of the shear strength of an anchor post-installed into masonry. Actually, those documents present only empirical formulations, some of them obtained by adjusting formulas derived for concrete, while analytical modeling is almost disregarded.

No analytical model can hence be borrowed from scientific or technical literature for the masonry shear strength, and what there is available it is adapted from other materials.

There are also reports and instructions edited by producers and manufactures that include formulas for predicting the shear strength of anchors embedded into masonry. Some of those formulas are implemented into software programs for practitioners. But the predictions of those formulas and that software are unrealistic, seeing that they are excessively low, which is something different than being conservative. Subsections 6.1 of this paper shows that those predictions are from three to twelve times lower than the actual shear strength and explains that underestimation is the unavoidable result of a mere empirical approach. If a designer uses those formulas or that software, the shear anchor does not turn out to be the best technical solution and not even a viable solution.

As a result, the designer who wants to employ shear anchors is almost obligated to perform on-site tests to directly measure the shear strength of the anchors included into his design. Indeed, the only topic that is

extensively covered by the mainstream papers is the definition of testing procedures [7,23,26,34,43,64], and the only topic that is adequately covered by codes and recommendations is the standardization of methods to test anchors for use in masonry or concrete [1,3,20,22,25,26,33,44,48,59].

In order to be statistically significant, however, on-site tests must be numerous. Unfortunately, the measure of anchor's shear strength is labor-intensive because it requires a sophisticated test set-up.

Moreover, if the test results are lower than the expected strength, the design must be changed, which entails serious problems for the designer, client, owner of the building, and construction activity, since the design change must be carried out at the construction site stage.

Eventually, the absence of an accurate predictive mathematical tool for the shear anchor embedded into masonry strongly affects structural activity dealing with existing buildings. It was due to exactly such problem found in his profession that the author of this paper set up this research program. Research includes both the single anchor and anchor groups, post-installed into either masonry or concrete. This paper is exclusively devoted to the single anchor post-installed into masonry and tackles the problem of analytically predicting anchor's shear strength.

Ultimately, the paper supplies an analytical formulation (composed of closed form mathematical expressions) that predicts anchor's shear strength. The presented model is the author's personal proposal to face and solve the problem, as no analytical approach can be taken or used from other research works, standards, or other sources.

1.6. General reference system, nomenclature, and stress sign convention

The reference structure is an anchor embedded into a semi-space (half-space). The half-space is made of masonry. The surface of the half-space is vertical and separates the masonry from the air. For the sake of clarity, it must be specified in advance that the model uses two different semi-spaces (half-spaces). One is that defined above, while the other is introduced in the following.

In the case of adhesive anchors, the schematic of the anchor includes the anchoring material, on the ground that these components have not to be differentiated from one another. Since those components and their mutual interface play no role, the paper often uses the term "anchor" for the whole embedded system.

The diagram of the reference structure is shown in Figs. 1 and 2; the former shows the ultimate behavior and the latter the internal forces acting on the embedded system.

The positions are described using a right-handed Cartesian coordinate system whose origin is on the surface of the semi-space (i.e., on the external surface of the masonry wall), at the center of the anchor (Fig. 3). The x-axis and y-axis lie on the external surface of the masonry wall; the former is horizontal, while the latter is vertical and its positive direction is downwards, according to the direction of the shear force. The z-axis is in the depth direction and its positive direction is from the masonry surface to inwards (Figs. 1 and 2).

The total length of the anchor is denoted by L (Fig. 2). One end of the anchor is embedded into the masonry (internal end), while the other end protrudes from the wall (external end), in order to allow the anchor to be connected to the steel plate. The distance between the external end and the masonry surface is denoted by e. The shear force V is applied at the external end. The shear force is hence applied with the eccentricity e to the masonry surface, i.e., with the lever arm e (Figs. 1 and 2). The eccentricity e incorporates both the distance of the shear force to the masonry surface and the couple transmitted by the attachment to the anchor (i.e., $V \times e$ must be equal to the bending moment acting at the section at $z = 0$, i.e., on the masonry surface). The embedded length of the anchor is hence $L - e$.

The diameter of the drilled hole is denoted by ϕ and the diameter of the anchor by Ω (Fig. 2). It follows that $\phi - \Omega$ is the gap between anchor and surrounding masonry, which is occupied by the anchoring material. If the anchor is installed without anchoring material, obviously $\phi = \Omega$.

Stresses are only considered as absolute values. Accordingly, the compressive stress in the model is assumed to be positive, while in the τ-σ plane is placed on the left part of the abscissa. For the sake of editing, some Greek symbols are written in Italic in the formulas but in normal character in the text.

2. Experimental campaigns performed to reveal the main events leading to the failure

The author was the structural designer and the works supervisor of five professional cases where he used steel shear anchors. Due to the absence of relevant code provisions, theoretical safety assessment (shear strength calculation) of the anchors that had been designed had to be

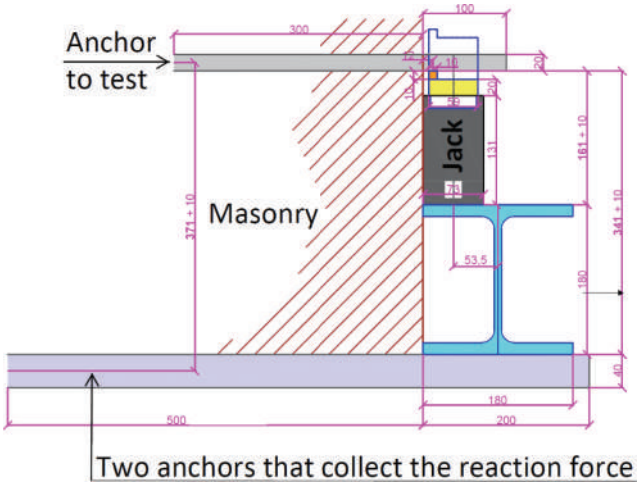

Fig. 4. Shear strength test set-up applied to the anchor having $\Omega = 20$ mm and $L - e = 300$ mm: Transverse section of the masonry wall and longitudinal section of the tested anchor. The jack (a cylinder with a head) applies the force to the bottom of the anchor through a steel element of square section, which reduces the eccentricity of the force. The figure also shows the I-section steel beam that collects the reaction force of the jack, which is supported by two anchors of large diameter and long embedded length.

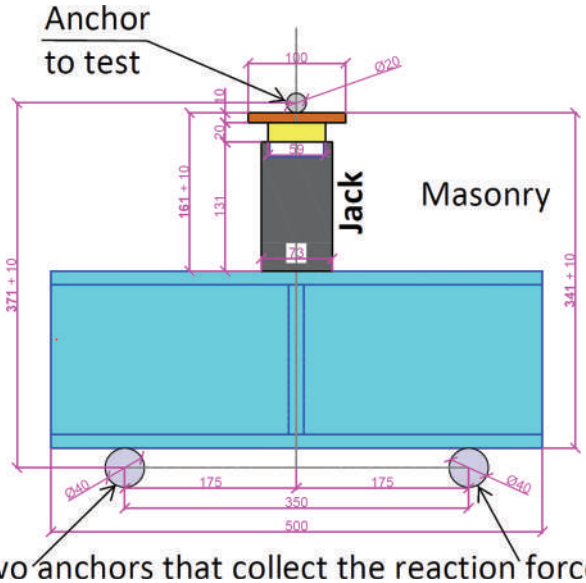

Fig. 5. Shear strength test set-up applied to the anchor having $\Omega = 20$ mm and $L - e = 300$ mm: frontal view. The jack pushes the steel bar (transverse to the tested anchor), which in its turn pushes the anchor's segment that protrudes from the masonry surface. The I-section steel beam that supports the jack is simply supported by the two lower anchors and is stiffened by a plate welded at the midspan. It is to note that the test set-up applies the force from downwards.

Fig. 6. Shear test performed using the procedure conceived and developed in this research activity. The masonry was made of bricks and lime mortar. Before executing this test, the plaster had been removed from the masonry. This test used the steel plate in lieu of the square-section steel bar.

confirmed by on site shear tests (Figs. 4 and 5). The professional cases were (Figs. 6-13): 1- the transformation of *Casa Suardi* in Bergamo (Italy) from a music school into a library, within the event "Bergamo Italian Cultural Capital for the year 2023"; 2- the repair, rehabilitation, and restoration of the *Fortress* (castle) in Reggiolo (near Reggio Emilia; Italy), 3- the restoration of *Villa Galvagnina* in Moglia (Mantua; Italy), 4- the structural retrofitting of the church *Santa Maria Assunta* in Riva del Garda (Trento; Italy); 5- the construction of a new multi-story building in Milan (Italy), in via San Martino 15.

In cases 1 and 2, new steel–concrete and steel-timber floors were connected to the existing masonry walls. The new primary steel beams were connected to historical brickwork, stonework, and mixed stone-brick masonry made of lime mortar. Each connection consisted of horizontal shear anchors post-installed into the masonry and bolted or welded to a steel plate which in turn was welded to the primary beam. Those anchors had hence to bear the vertical design loads acting on the new floors (Figs. 6, 7, 9-11).

In case 3, the existing floors were connected to the supporting masonry walls because the existing connections were damaged or ineffective. More specifically, the primary timber beams were connected to historical walls made of a very poor masonry, composed of handmade bricks and weak lime mortar. Each connection consisted of horizontal shear anchors post-installed into the masonry and bolted or welded to a steel plate, which in turn was bolted to the existing timber beam. Here too, the anchors had to bear the vertical design loads acting on the floor (Fig. 8).

In case 4, the existing structures of the roof of the nave and the two aisles were connected to the supporting masonry walls. More specifically, the primary and secondary timber beams of the roof were connected to historical masonry walls made of stone and lime mortar. Each connection consisted of horizontal shear anchors post-installed into the masonry and connected to the timber elements by a special device that allowed the timber to shrink and expand (Fig. 12).

In case 5, some parapets of a new building were connected to non-structural external walls. More specifically, glass parapets were connected to walls made of perforated (hollow) bricks and cement mortar.

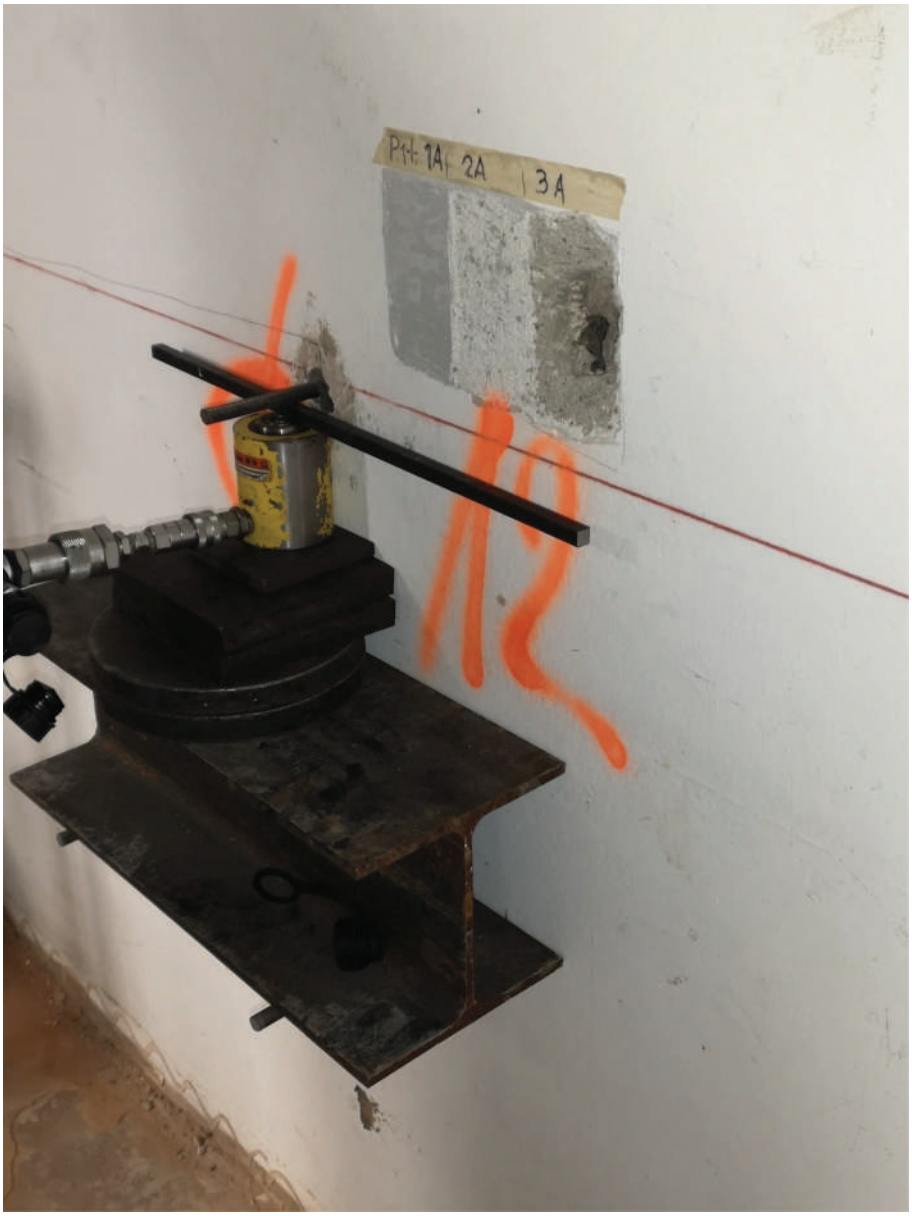

Fig. 7. Shear test performed on an anchor embedded into a masonry made of stones and lime mortar. In this test the plaster had not been removed because it consisted of a thin film. So, on one hand, the plaster did not alter the behavior of the anchor, while on the other hand, it allowed the cracks to be better observed and identified.

Each connection consisted of a horizontal shear anchor embedded into the perforated masonry and joined to the steel frame of the glass parapet. Given that the bricks were perforated, each anchor was enveloped by a sock, so that the resin only filled the space between the anchor and the sock without penetrating the hollow bricks. The anchors of each parapet had to bear the horizontal design loads. The tests of these anchors were performed by using a set-up different than that used for the other four cases (Fig. 13).

The writer of this paper designed and then directed the experiments. Eventually, the author analyzed and interpreted the experimental results that had been collected.

Those experiments aimed not only to verify that the shear capacity of each anchor was greater than the relevant demand, but also to observe the main events leading to failure of an anchor embedded into masonry, and to comprehend its ultimate behavior.

Those tests and their results represent a wealth from two points of view – namely, a wealth in terms of knowledge, due to the gap in literature pointed out in Subsection 1.5, and a wealth in terms of economic value, as those tests cost a great amount of money.

2.1. Test method and test set-up

On-site shear test of anchors poses two crucial demands for the experimenter. The first is to resist the reaction force of the jack. In the case of the pull-out test the reaction force, which is perpendicular to the masonry surface, is resisted by the masonry, so the test does not require any specific set-up. Conversely, in the case of the shear test, the reaction force, which is parallel to the masonry surface, needs to be collected by a specific set-up.

The second demand is to reduce the eccentricity of the shear force as much as possible, in order to prevent the anchor's cross-section at the masonry surface from collapsing due to excessive bending moment. The real value of the eccentricity, which however cannot be nullified, must be known, in order to interpret the results.

Fig. 8. Photo taken after having completed the test and having taken away the test set-up. The image shows the anchor just tested, which is bent upward, and the two lower anchors, which supported the steel beam and the jack during the test. On the top right the photo also shows the two flat jacks that had been used to measure the compressive strength of the masonry.

The author satisfied those demands by designing a specific test set-up. That (Figs. 4 and 5) set-up is applicable and useful for shear testing any anchor. As such, it is also proposed for further experimental research regarding shear anchors, both in and outside the academia. As a matter of fact, the author uses that test set-up in his professional activity and will use it to extend this research work to anchor groups and to anchors embedded into concrete structures.

The test set-up is comprised of a hydraulic jack, including the control unit, two adhesive anchors, a steel beam of I-section, a tiny steel bar of square section, and two displacement transducers.

The first step of the testing procedure is to post-install the anchor that will be tested and two other anchors into the masonry, the former above and the latter below at the same height. After the anchoring material has cured, the steel beam is placed onto the two anchors. Then the jack is placed between this steel beam and the anchor to be tested, supported by the former and connected to the latter by means of the steel bar having tiny square cross-section (Figs. 4 and 5). The shear force is applied by the jack to the anchor to be tested through that steel bar, which concentrates the force onto a small area of the protruding anchor's length, so as to have only a small eccentricity. During a test, hence, the two anchors support the steel beam, which in turn supports the jack that pushes from below the anchor to be tested.

The greater the capacity of the jack the grater its size and, in turn, the greater the eccentricity that it implies. Thus, three types of hydraulic jacks were used, depending on the strength that was expected – namely, a 100.0 kN jack, a 300.0 kN jack, and a 500.0 kN jack. Those jacks guaranteed a great accuracy in controlling and measuring the applied force.

The two inferior anchors and the steel beam were dimensioned to bear the reaction of the jack and to exhibit negligible deflections during the tests. The diameter of the two anchors was large (42 mm each), and their embedded length long (500 mm each). Moreover, the steel beam was stiff (an HE180B European section), and the span between the two anchors was short (350 mm).

Fig. 9. Photo taken when the anchor had just collapsed. The image shows the test set-up and the tested anchor, which is bent upward. In all the tests the anchor reached rotations substantially larger than that induced by the peak of the force, with no more than moderate decrease in the force applied by the jack (pseudo-plastic post-peak behavior).

Ultimately, the anchor to be tested was by far the weakest and softer (most flexible) component of the system. In so doing, the failure mode of the anchor was pure shear.

The steel bar, whose cross-section was 10 × 10 mm, made the eccentricity of the applied force be 5 mm, which is sufficiently small. However, during the test with the greatest jacks, that bar tended to slide. Therefore, it was replaced by a thick steel plate, which kept the eccentricity 5 mm.

The displacement transducers were placed one at the section of the anchor that emerged from the masonry surface and the other at the free end of the anchor (external end). In so doing, the rotations could be measured as well.

2.2. Shear tests

Every masonry portion where an anchor was post-installed, had been previously tested in order to know its mechanical characteristics. Each masonry portion was tested by performing a double flat-jack test (Figs. 8 and 11), a shove test, and, in the case of stonework masonry, a diagonal compressive test. The double flat-jack test provided the uniaxial compressive strength of the masonry (the ultimate one-dimensional stress), which is one of the data to plug into the model. The shove test and the diagonal compressive test provided the friction angle of the masonry, which is the other data relevant to the masonry to plug into the model. Every tested anchor was embedded in a position sufficiently far from the portion of masonry that had been tested in order to measure its mechanical characteristics, so as not to suffer from any disturbance due to the previously performed tests.

Each experiment tested an anchor that had been purposely designed. The tested anchors covered typical scenarios; were post-installed into almost all the masonry types that can be found in historical buildings and were bonded using all the possible techniques. More specifically, the anchors were installed into brickwork, stonework, and mixed stone-brick masonry, and were bonded to masonry with either resin or

Fig. 10. Typical crack pattern at collapse. In every test when the anchor reached the maximum shear force that it could bear (failure), a vertical crack triggered at the upper point of the circular boundary of the drilled hole. Each test was continued increasing the anchor's rotation (and slightly decreasing the force applied by the jack). When the rotation increased, that crack propagated vertically upwards into the masonry. Then, other cracks triggered, with initiation at the upper semi-circumference of the drilled hole and with radial upwards propagation. In all the tests, the behavior softened only after rotations significantly larger than that at the maximum force (i.e., at the peak of load).

mortar, or otherwise with no anchoring material (Figs. 6-13).

In each test the force applied by the jack to the tested anchor was increased from zero up to the complete collapse of the anchorage. Every test measured the maximum shear force that the anchor could bear (ultimate shear force) and the load–displacement relationship. Ergo, every test provided the shear strength of the tested anchor, and at each step of load both the deflection of the anchor's section at the masonry surface and the rotation angle.

The load process included some unloadings; the force of the jack was taken away and then a new loading was started. In so doing, the elastic limit of the anchorage was identified.

2.3. Experimental campaigns and outcomes

As anticipated in the incipit of Section 2, in cases 1–4 the anchors were installed into ancient masonry walls. So, the joints were made of lime mortar, the brickwork of handmade bricks (produced before the Hoffman kiln), and the stonework of rough-cut stones with an irregular stone pattern. In cases 5 the anchors were installed in a masonry made of hollow (perforated) bricks.

Thirty-six experiments were performed, which can be subdivided as follows (Table 1): 13 anchors embedded into brickwork, 14 into stonework, 7 into mixed brick-stone masonry, 2 into hollow bricks.

The following geometries were tested: drilled hole diameters from 13 mm to 44 mm; embedded lengths from 100 mm to 400 mm; eccentricity 5 mm. Both adhesive and mechanical anchors were tested. For the adhesive anchors, both resin and mortar anchoring materials were used. Three types of resins and three types of mortar were used – namely, one strong and stiff product, a relatively weak and soft product, and a product whose mechanical characteristics were intermediate (average stiffness and strength).

Some of the shear tests that were performed are shown in Figs. 6-14. The test results obtained from the five experimental campaigns (case studies 1–5) are reported in Table 1, which, for each experiment, tabulates: the geometric parameters of the anchor, the mechanical characteristics measured for the masonry that the anchor was embedded into, the measured shear strength, denoted by $V_{u\text{-}ex}$ (i.e., the maximum force reached by the jack), and the measured pseudo-elastic limit shear strength, denoted by $V_{e\text{-}ex}$ (i.e., the force of the jack beyond which some residual deformations were observed and that caused a sudden

Fig. 11. Shear test performed in the case of a masonry made of bricks and stones, with lime mortar. The anchor was embedded into a stone of large size. The photo was taken after the test. The image shows the anchor just tested, which was bent upward, and the two lower anchors, which supported the steel beam and the jack. The upper part of the masonry (without plaster) had been tested in order to measure the mechanical characteristic of the masonry.

reduction in stiffness).

Figs. 15 and 16 show the load–displacement curves of two tests and the relevant load-rotation curves, respectively. Those curves are representative of all the experiments performed. The load (on the ordinate) is the shear force applied by the jack. The displacement (on the abscissa) is the vertical translation of the point of the masonry surface at $x = 0, y = \phi/2, z = 0$. The rotation (on the abscissa) is that of the segment of the anchor which protrudes from the masonry surface. For the anchors that did not yield and however before the yielding of the anchor's section at the masonry surface (after which the segment exhibited a local plastic bend), that rotation coincides with the rotation of the anchor inside the masonry (Fig. 14).

Fig. 15, as well as all the other 34 load–displacement curves, shows a significant elastic behavior, followed by an elasto-plastic and then a plastic behavior which are as much significant. Moreover, Fig. 15 and all the other curves show both large ultimate displacement and large plastic deformation (rotation).

The last two tests of Table 1 used a different set-up (Fig. 13). The shear force was applied by a jack that pulled the anchor by means of a steel cable restrained by a crane. In Fig. 13 the photo on the right was taken just after the anchor had reached the complete collapse.

3. Experimental results

The forces resisted by the anchors and the load–displacement curves are important results (Table 1; Figs. 15 and 16). However, the main outcome was that the shear anchors embedded into masonry share the same qualitative behavior. The tested anchorages were significantly different from each other, since the anchors both ranged from small to large in diameters, and from short to long embedment lengths. Moreover, the anchors were embedded into brickwork, stonework, and mixed stone-brick masonry, using different types of anchoring materials. Despite the great variety among the anchorages, the tested anchors exhibited the same mode of failure and the same events leading to

Fig. 12. Case study 4. Anchors after having reached collapse. This anchor was a rebars of diameter 200 mm. In this test the plaster could not be removed because of its high cultural and artistic value.

Fig. 13. Case study 5. This experiment was borderline, as it tested anchors post-installed into a masonry made of hollow bricks (perforated bricks, shown by the photo on the right), which required each anchor be enveloped by a sock.

Table 1
Experimental results and relevant model predictions. The 1st column specifies the type of masonry: bl = brickwork with lime mortar; sl = stonework with lime mortar; sb = mixed masonry work of stone and some bricks, with lime mortar; bc = perforated brickwork with cement mortar. The 2nd and 3rd columns report the mechanical characteristic of the masonry provided by the on-site tests. The column from 4th to 7th provide the geometrical characteristic of the anchorage, where $L_e = L - e$. The 8th column indicates the type of bond: SR = soft resin anchoring material; AR = average resin anchoring material; RR = stiff resin anchoring material; SM = soft mortar anchoring material; AM = average mortar anchoring material; RM = stiff mortar anchoring material; McA = mechanical anchor. The 9th column reports the measured shear strength of the anchor, $V_{u\text{-}ex}$. The 10th column reports the measured pseudo-elastic limit value, $V_{e\text{-}ex}$. The 11th column (2nd to last column) reports the anchor's shear strength provided by the model, V_u. The 12th column (last column) reports the elastic limit provided by the model, V_e.

	f_m	μ	ϕ	L_e	Ω	e	Bond	$V_{u\text{-}ex}$	$V_{e\text{-}ex}$	V_u	V_e
	N/mm^2	/	mm	mm	mm	mm	/	kN	kN	kN	kN
bl	6.13	0.61	20	200	18	74	SR	17.30	11.26	16.464	10.304
bl	6.13	0.61	20	200	18	74	AR	17.91	11.32	16.464	10.304
bl	6.13	0.61	20	200	18	74	RR	17.99	10.98	16.464	10.304
bl	6.13	0.61	20	200	12	74	SM	16.01	10.01	16.464	10.304
bl	6.13	0.61	20	200	12	74	AM	18.04	11.59	16.464	10.304
bl	6.13	0.61	20	200	12	74	RM	16.50	10.41	16.464	10.304
bl	6.13	0.61	20	200	20	74	McA	15.40	9.77	16.464	10.304
sb	5.32	0.54	28	300	24	74	SR	32.04	19.03	31.513	19.548
sb	5.32	0.54	28	300	24	74	AR	33.17	20.73	31.513	19.548
sb	5.32	0.54	28	300	24	74	RR	34.71	21.16	31.513	19.548
sb	5.32	0.54	28	300	18	74	SM	31.26	20.99	31.513	19.548
sb	5.32	0.54	28	300	18	74	AM	29.09	20.54	31.513	19.548
sb	5.32	0.54	28	300	18	74	RM	33.79	21.12	31.513	19.548
sb	5.32	0.54	28	300	28	74	McA	30.30	17.61	31.513	19.548
sl	7.77	0.69	40	400	26	29	AM	165.65	102.18	132.518	82.543
sl	7.77	0.69	36	400	22	29	AM	146.52	90.63	120.096	74.289
sl	7.77	0.69	30	380	20	29	AM	112.38	69.04	95.240	58.510
sl	7.77	0.69	26	350	18	29	AM	93.13	56.05	75.569	46.298
sl	7.77	0.69	26	320	16	29	AM	81.91	50.00	70.782	43.514
sl	7.77	0.69	24	260	14	29	AM	57.29	35.49	49.391	30.577
sl	7.77	0.69	16	180	12	29	AR	25.13	16.02	21.482	13.267
sl	7.77	0.69	14	165	10	29	AR	20.19	12.70	16.973	10.457
sl	7.77	0.69	12	150	10	29	AR	13.81	9.09	12.992	7.981
bl	2.12	0.23	27	270	18	74	AM	8.43	4.75	7.981	4.979
bl	2.12	0.23	25	230	18	29	SM	7.61	4.77	7.436	4.660
bl	2.12	0.23	23	190	18	29	SM	5.57	3.62	5.409	3.427
bl	2.12	0.23	18	160	14	29	SR	3.75	2.22	3.470	2.182
bl	2.12	0.23	15	125	12	29	SR	1.99	1.21	2.115	1.340
bl	2.12	0.23	13	100	10	29	SR	1.34	0.90	1.362	0.873
sl	10.59	0.64	32	500	24	74	SM	178.07	107.07	148.778	90.603
sl	10.59	0.64	32	450	24	74	SM	155.94	94.91	130.788	79.930
sl	10.59	0.64	22	350	18	74	SM	78.72	47.54	66.435	40.453
sl	10.59	0.64	22	280	18	74	SM	58.58	35.70	49.664	30.525
sl	10.59	0.64	22	240	16	74	SM	47.03	28.38	40.252	24.983
bc	1.39	0.25	14	250	12	25	RR	2.91	1.76	3.213	1.951
bc	1.11	0.21	14	250	12	25	RR	2.85	1.67	2.494	1.514

failure. According to the experimental observation, hence, the geometry of the anchorage and the mechanical characteristics of the masonry impact only on the value of the shear strength but neither on the mode of failure nor on the behavior by which the shear strength is achieved. That experimental result has allowed an analytical predictive model to be constructed.

The shear force applied by the test set-up to the tested anchors was directed upwards (for safety reasons during operation), while the shear force applied by an attachment to an anchor is directed downwards. As explained in the following, the direction of the vertical shear force has no influence. For the sake of avoiding confusion, the analysis of the experimental results takes the positive direction of the y-axis as upwards (the Cartesian coordinate system shown in Figs. 2 and 3), i.e., to be that of the shear force applied in the experiments.

3.1. Behavior shared by all the anchorages, analysis, and interpretation

The experiments have shown that the embedded length of every anchor underwent a rigid body motion during the entire test, from the beginning up to the ultimate strength of the anchor (Figs. 8, 9, 11-13). Accordingly, when the shear force increased from zero up to failure, each anchor translated vertically and rotated in the vertical plane it lies on, i.e., in the y-z plane (Figs. 2 and 3). The experiments have also shown that no measurable or visible relative movement occurred between anchor and drilled hole. The anchoring material undergoes hence a rigid body motion as well. Ultimately, anchor and anchoring material (the embedded system) exhibited rigid body motion up to failure.

Not only was that behavior proven by the displacements recorded by the transducers, but also was shown by every anchor extracted from the masonry after the test, seeing that the deviation from rectilinearity of every anchor's embedded length was always negligible (Fig. 14).

The ratio between the length L and the diameter Ω of all the tested anchors, called slenderness ratio, fulfilled the inequality $L/\Omega \leq 26$. Moreover, the gaps ϕ – Ω respected the limits of Subsection 1.3. Thus, a slenderness ratio lower than (or equal to) 26 and a thickness of the anchoring material in compliance with the provisions of Subsection 1.3 guarantee a rigid body behavior of the anchor.

The displacement of an anchor measured at a load step by the transducer at the external end minus that measured by the transducer at the masonry surface divided by e is the trigonometric tangent of the anchor's rotation angle of the segment e, at that load step. At the load steps in which e did not exhibit any plastic deformation (almost up to failure), that angle coincided with the rotation angle of the embedded length. The experimental information included hence the fractions of anchor's displacement due to its rigid rotation and its rigid translation. The latter was found to be ever negligible with respect to the former (Fig. 1).

Ultimately, a shear force produces a rigid roto-translation of the embedded length, but the rigid body vertical translation of the anchor can be ignored compared with the linearly varying vertical

Fig. 14. Four anchors of different diameters and lengths, extracted from the masonry after the tests. All the anchors extracted from the masonry after the tests did not exhibit any plasticity in the embedded part (while the sections that emerged from the masonry surface exhibited large residual bending).

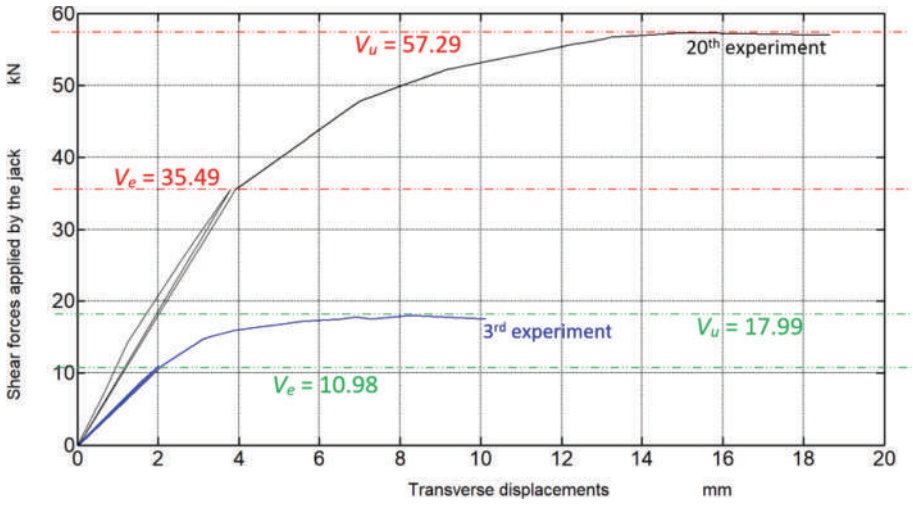

Fig. 15. Load-displacement curves of the 3rd and 20th experiments of Table 1. Abscissa: vertical displacements of the anchor's cross-section at the masonry surface. Ordinate: transverse forces applied by the jack to the anchor. The descending branch of the curve was not represented, as it strongly depended on the way the jack was extended. The figure also shows V_u and V_e.

displacements produced by the rigid body rotation (Fig. 1). In brief, a shear force induces a rigid rotation of the anchor.

That result about the absence of measurable or visible deformation in the entire embedded system is in agreement with another result of these experiments. The shear strength of the anchor was proven to be independent of presence and type of anchoring material. The facts that the anchoring material be resin or mortar, stiff or soft, present or absent (adhesive or mechanical anchors) play no role in the shear strength of the anchor.

Those results anticipate another experimental result. In every test the mode of failure was dictated by the rupture of the masonry surrounding the anchor, while the embedded length of the anchor was still in the elastic field (Figs. 9-11). More specifically, the anchor and anchoring material reached no more than small strains compared with their elastic limit, while the masonry around the anchor reached high strains, which caused that masonry to fail.

Those experimental observations are also in line with the rectilinearity of the embedded length that was observed for every anchor extracted from the masonry after the test (Fig. 14). In fact, the rectilinearity demonstrated, not only the rigid motion, but also the absence

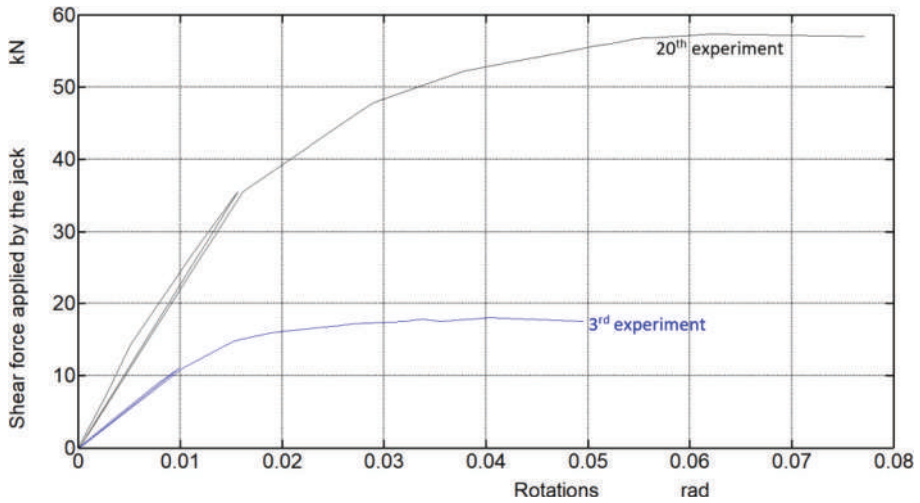

Fig. 16. Load-rotation curves of the 3rd and 20th experiments of Table 1. Abscissa: rotations of the part of the anchors that protrudes from the masonry surface. Ordinate: transverse forces applied by the jack to the anchor.

of plastic deformations in the embedded length of the anchors; every anchor remained in the elastic field up to failure, so the shear strength was not dictated by the anchor.

Regarding the segment e that protruded from the masonry, it was subjected to bending moment due to the eccentricity of the shear force. In some anchors, that bending moment bent the segment e beyond the elastic limit, but without reaching the ultimate bending moment (strain hardening behavior of the steel). All the anchors maintained hence their capability to transfer the shear force to the masonry up to the complete collapse of the surrounding masonry, although some protruding segments were visibly bent.

Elaborations of the experimental results demonstrated that in many cases the extra-strength provided by the bending of the segments e is no more than moderate. That extra-strength can therefore be neglected and left to a more sophisticated model. Accordingly, the anchor can be assumed to be infinitely rigid (the entire length L, not only the embedded length $L - e$).

The tests included some unloadings of the force applied by the jack. From a certain force onwards, the embedded length of the anchor did not return to its original position when the force was taken away. That force defined the elastic limit of the shear behavior.

By definition, increasing the force applied to the anchor beyond the elastic limit caused a progressive decreasing in the stiffness of the anchorage. That is, equal steps of load beyond the elastic limit produced progressively greater displacements. That progressive decrease in stiffness was not caused by any visible crack; it was therefore the result of non-linear behavior of masonry (pseudo-plasticity).

The increase in shear force and the consequent decrease in stiffness led the stiffness to approach zero. The force that made the stiffness be zero was the maximum shear force that the anchor could bear. Ergo, that force was the shear strength of the anchor. In fact, a further increase in the applied force could not be resisted by the anchor, being that the anchorage had entirely lost its stiffness and had become an unstable structure against increments in load. The condition in which the applied force was the maximum and the stiffness was zero, was hence the ultimate limit state of the tested anchor.

In every experiment, the rotation attained by the anchor at the ultimate limit state was found to be appreciably greater than the elastic limit rotation (Fig. 16).

No crack was observed until not only the anchor's shear strength was reached, but also the ultimate rotation was appreciably surpassed (Figs. 6-13). Getting more into detail, collapse ever started with the rupture of a point on the masonry surface whose coordinates were $x = 0$, $y = +\phi/2$, and $z = 0$. That is, the rupture occurred at the point where the anchor induced the greatest normal compressive strain. That event initiated the post-failure behavior of the anchor, i.e., changed the slope of the load-displacement curve, however without appreciably reducing its derivative. The analysis of the experimental results demonstrated that the rupture of that point occurred for strains substantially greater than the elastic strains corresponding to the maximum combination of σ and τ.

After ultimate of every test the jack kept pushing against the anchor, although with a lower force. In so doing, the rupture continued in the masonry aside that point, along the entire semi-circumference of the drilled hole where the rupture had started (x from $-\phi/2$ to $+\phi/2$, y from $+\phi/2$ to 0, $z = 0$). The propagation of the rupture gave rise to pseudo-vertical cracks in the masonry surrounding that semi-circumference (Figs. 10, 12).

Those cracks decreased substantially the stiffness of the system, but reduced only marginally the capacity of the anchor to bear shear force. That result was understood after having analyzed the stresses in the masonry, which were found to be a two-dimensional compressive stress state, without any tensile stress (Fig. 2 shows that all stresses are compressions and that they do not vary with z). The cracks were hence parallel to the contact pressures. Ergo, those cracks did not cause any contact pressure to disappear.

The ultimate rotation could thus be increased to a certain degree without causing any appreciably decrease in the force applied by the jack. The peak force dropped down only when the cracks propagated completely in the surrounding masonry, which required a rotation substantially greater than the ultimate rotation.

Those experimental outcomes demonstrate that the masonry around the drilled hole can display large plasticity. In particular, the masonry surrounding the drilled hole can exhibit a plasticity that is much greater than the plasticity exhibited by the same masonry subjected to a one-dimensional stress state. That was one of the main results of the experimental activity, as it allowed the model to be based on the resultant forces instead of the strains (Fig. 2).

Each experiment included the single flat jack test, which measured the stress in the masonry prior to the installation of the anchor. The correlation between the experimental results demonstrated that the anchor's shear strength does not depend on the stress state that existed in the masonry prior to the installation of the anchor. E.g., in the experiments 1, 3–5, 8, 12–14 of Table 1, the stresses were high, while in the experiments 2, 6, 7, 9–11 were low. The reason is that the drilled hole gives rise to an arch effect that unloads the masonry around the anchor. The masonry that surrounds the anchor reaches therefore failure only due to the stresses and strains induced by the anchor. It follows that

a downwards shear force produces the same response as an upwards shear force.

The experimental results have proven that the shear strength and structural performance of an anchor depend on the diameter ϕ of the drilled hole, but not on the diameter Ω of the anchor. That outcome can be confirmed by comparing to each other the experiments 1–7 of Tab 1, or the experiments 8–14. The gap between anchor and drilled hole plays hence no role in the ultimate behavior of the anchor.

The correlations between the thickness of the walls and the response of the anchors showed that the latter does not depend on the former. Definitely, the experimental results demonstrated that neither how much the wall thickness surpasses the embedded length $L - e$ nor the ratio between wall thickness and embedded length influences the shear capacity of an anchor. It can thus be inferred that the shear strength of the anchor is not dictated by the z-stresses. Ergo, the stress state that governs the behavior of the anchor is two-dimensional.

The elaborations of the experimental results confirmed that anchor's failure depends on the major principal stress σ_1 and the minor principal stress σ_2 acting in the vertical plane x-y, while it does not depend on the principal stress σ_3 acting out of the x-y plane.

In some tests (the experiments 6, 11, and 26 of Table 1), the masonry wall exhibited a local failure mode which consisted in the flaking off of the masonry surface (masonry spalling). Masonry spalling is the separation (detachment) of a layer (a piece) of masonry from the main structure. The initial stage of this failure mode consisted of surface cracks in the masonry (parallel to the masonry surface) caused by the stresses acting on the circular external contour of the drilled hole or on a corner of the block the anchor was embedded into. With the increasing of the shear force, those cracks resulted in the breakdown of the masonry, which consisted in the detachment of a layer or a wedge of the block from the wall. That failure mode, which is here called "block surface failure" (Subsection 5.3), is shown in [62,63].

3.2. Contact pressures acting on the drilled hole

The experimental results demonstrated that the behavior of the anchor is governed by the contact pressures acting along the entire embedded length of the anchor.

Figs. 1 and 2 show the center of the rigid rotation at the ultimate displayed by the anchor. Accordingly, the drilled hole can be split into two cylinders, the first from the masonry surface to the rotation center, and the second from the rotation center to the internal end. Each cylinder can be envisioned as composed of two half-cylinders, symmetric with respect to x. Regarding the first cylinder, the anchor presses against the half-cylinder with positive y-coordinates and pulls the complementary semi-cylinder with negative y-coordinates. Regarding the second cylinder, the anchor presses against the half-cylinder with negative y-coordinates and pulls the complementary semi-cylinder with positive y-coordinates (Fig. 3).

The push of the anchor against the half-cylinders generates compressive stresses which consist of contact pressures (Fig. 1). The interface between anchor and masonry transmits therefore contact pressures, which are vertical (y-directed), and are smeared both along the entire length (z-axis) and across the entire width (x-axis) of the two above defined half-cylinders. The contact pressures acting onto the masonry of the first half-cylinder are directed towards the positive y, while those acting onto the masonry of the second half-cylinder are directed towards the negative y (both of them consists of σ_y, as they act on planes whose normal is in the direction of y). Obviously, the same contact pressures with opposite direction act onto the anchor. In fact, the shear force is equilibrated by the contact pressures acting onto the anchor. So, the shear strength of the anchor V_u is the shear force equilibrated by the contact pressures at failure.

The contact pressures are denoted by p_c (Fig. 3). The contact pressures at failure are denoted by q_{mc}. The use of q in lieu of p aims at indicating that the contact pressures at failure are not only pressures but also the load (symbol q) acting on the masonry that causes the masonry to fail and, as such, dictates the shear strength of the anchor.

The pull of the anchor from the complementary half-cylinders, in the case of adhesive anchors, induces tensile stresses in the masonry behind the relevant half-cylinders (Fig. 1), which cause that masonry to crack. Eventually, those cracks make the tensile stresses disappear, and the anchor detaches from those half-cylinders. In the case of mechanical anchor, the pull makes immediately the anchor detach from the relevant half-cylinders.

4. Mechanical assumptions of the model based on experimental observations

The experimental results support and justify the following four assumptions, which exhaustively describe the mechanics of the shear anchor and, as such, allow for modeling its ultimate behavior.

1. The embedded system undergoes only rigid body rotation.
2. The stress state in the masonry that surrounds the anchor is produced only by the compressive contact pressures induced by the anchor.
3. Block surface failure consists in a reduction of the embedded length equal to the thickness of the layer that has detached, which is here denoted by c.
4. The stress–strain law of the masonry that surrounds the drilled hole is elastic-perfectly plastic.

Assumption 1 implies that the embedded length of the anchor and anchoring material remains straight (rectilinear) under load, up to the collapse. The strains in the anchor (and in the anchoring material) can therefore be neglected.

That assumption does not depend on the mechanical characteristics of masonry and holds true at least for slenderness ratios $L/\Omega \leq 26$ and gaps $\phi - \Omega$ that respect the limits of Subsection 1.3.

That assumption is necessary only for the elastic model but not for the ultimate model. Nevertheless, it simplifies the presentation (Assumption 4 implicitly contains Assumption 1).

Assumption 2 means that the stresses due to loads different than the shear force are neglected. The stresses due to the dead and live loads of the building are therefore ignored.

It follows that the position within a homogeneous masonry at which the anchor is installed plays no role in the ultimate behavior (at the base or at the top of a wall is the same).

Moreover, Assumption 2 allows the tensile contact pressures to be neglected. It follows that the strength of the anchor derives from the contact pressures that press against the two half-cylinders (Subsection 3.2), while no contact pressures that pull the complementary half-cylinders are accounted for in the model.

Assumption 3 establishes that block surface failure does not prevent the anchor from resisting shear forces greater than that which has triggered this failure mode, but simply the layer that has detached does not transfer any contact pressure. As such, block surface failure is a local failure mode which does not dictate the shear strength of the anchor. The Cartesian coordinate system is placed on the masonry surface after block surface failure, if it were to happen.

The model allows the user to choose whether to include or not the occurrence of that failure mode. In the former case, the effective embedded length is $(L - e - c)$, while in the latter case is $(L - e)$. The equations are written using a value of c that is in proportion to ϕ, but the model allows the user to employ a different value of c.

Assumption 4 accurately describes the inelastic behavior of a confined masonry. In fact, confinement (i.e., σ_2: see Subsections 3.1 and 3.2) boosts the plastic response of the material.

Perfectly plasticity means not only that the stress does not change during the plastic strain increments, but also that plasticity is unlimited. A plasticity without any strain limit implies that failure is reached when a sufficiently large portion of masonry reaches the ultimate compressive

stress, while the strains cannot break the masonry, as well as local stresses cannot trigger the failure.

Ergo, q_{mc} is the maximum contact pressure that can be reached by the masonry around the anchor (ultimate contact pressures), not the contact pressure that causes masonry to break.

According to the above fact that the strains play no role in shear capacity, the contact pressures at ultimate limit state are uniformly distributed over the width and length of the drilled hole. Hence, q_{mc} is uniform along the width ϕ. Moreover, q_{mc} is uniform along the lengths of the two half-cylinders, apart from two segments around the rotation center, where the contact pressures are elastic, and apart from the thickness c. The ultimate contact pressures q_{mc} are directed either upwards or downwards, depending on the half-cylinder that they act onto.

Ultimately, Assumption 4 implies that the contact pressures at failure are two strip loads of width ϕ, different length, and opposite direction.

Those longitudinal distributions in turn entail that the stresses induced by the contact pressures in the masonry can be well approximated by a plane stress state (a two-dimensional stress state). It is to note that the plane stress state is also in agreement with the independence of the ultimate behavior on the masonry beyond the internal (embedded) end that was found in the test. In fact, the experimental results have proven that there is no interaction between the vertical layer of wall where the anchor is embedded (whose thickness is $L - e$) and the adjacent vertical layer of wall.

Anyway, the strains reach the maximum in the plane at $z = 0$ (external masonry surface), where σ_z, τ_{zx}, τ_{zy} are zero, which further strengthens the validity of assuming that the stress state is plane.

Ultimately, a corollary of Assumption 4 is that the q_{mc} - value of the contact pressures results from a plane-stress state, while it does not depend on the out-of-plane stresses.

The contact pressures acting on two segments around the rotation center, whose lengths are denoted by a and d, are elastic; so, they range from zero at the rotation center to q_{mc} at the distances a and d from the rotation center.

The final equations are written using values of a and d that are in proportion to ϕ, derived from the average rotation at the ultimate observed in the experimental campaigns. But the model allows the user to employ different values of a and d if a different ultimate rotation is expected. The elastic contact pressures acting on a and d are ignored, since their contributions are negligible.

5. Analytical model for anchor shear strength prediction

The model consists of a two-step process in which first the contact pressures at failure q_{mc} are defined, and then the shear strength of the anchor V_u is predicted.

5.1. Ultimate contact pressures q_{mc}

This subsection presents the first step of the process. Assumptions 1 and 4 (Section 4) imply that the mode of failure of the shear anchor is the kinematic rotational mechanism. Given that a kinematic mechanism is an unstable structural configuration, the shear strength of the anchor can be obtained from the sole equilibrium equations. Those equations require defining the value of the contact pressures that trigger the failure of the masonry, q_{mc}, which is what this paragraph is devoted to. This subsection refers only to the contact pressures acting on the drilled hole, not to those equal and opposite acting on the anchor.

Assumption 4 allows for obtaining the contact pressure at failure q_{mc} by virtue of its corollary, which establishes that the shear force induces a plane stress state.

The model that best describes that two-dimensional stress state is the homogeneous, isotropic, weightless, linearly elastic half-space with a plane horizontal surface at $y = \phi/2$, loaded at that surface. That half-space extends beyond the origin towards the negative z, and beyond the embedded end (the portion of the half space whose z coordinates are outside the anchor length plays no role).

It is essential to realize that this half-space is not the semi-space introduced in Subsection 1.6. The latter represents the masonry the anchor is embedded into, and its surface lies on the x-y axes (vertical plane) at $z = 0$, while the former (the half-space introduced here) represents the masonry that the compressive contact pressures act onto, and its surface lies on the x-z axes (horizontal plane), tangent to the drilled hole.

The plane stress state together with the constant magnitude of the contact pressures at failure q_{mc} imply that the loading that best describes the anchor's ultimate behavior is the uniform strip load having magnitude q_{mc}, infinite length along the z-axis, and width ϕ along x-axis, applied at the plane horizontal surface of the half-space (Fig. 3). The half-space and the strip load describe the behavior of both the masonry subjected to downwards contact pressures and to upwards contact pressures, given that the stress state depends only on the contact pressures acting at z.

The positions in the x-y plane are identified by the coordinate α, which is alternative to the Cartesian coordinate system (Fig. 3). Of course, α cannot identify a single point of the x-y plane, but it identifies a curve. The α-coordinate allows the width ϕ to be eliminated, since ϕ is included into α.

Equations for stresses and strains induced in this half-space by a point load perpendicular to the surface and acting at the surface were first obtained, in usable form, by Boussinesq (1885) [67–69]. That model is linear. The stresses and strains for other loads can thus be calculated by applying the principle of superposition. The two-dimensional stress state induced by the anchor in the masonry was hence obtained by integrating a well-known analytical equation.

The highest and lowest principal stresses of the plane stress state are hereinafter denoted by σ_1 and σ_2, respectively. The third principal stress σ_3 is equal to σ_z, and therefore is zero. Both σ_1 and σ_2 resulted to be compressions at every point of the half-space. That result is fundamental; it shows that the shear strength of an anchor is dictated by masonry compressive strength and not by masonry tensile strength. Accordingly, the former is a free parameter of the model, while the latter plays no role.

The absolute value of the major principal stress σ_1 at failure as a function of α, is the compressive stress:

$$\sigma_1 = \frac{q_{mc}}{\pi}\cdot[\alpha + \sin(\alpha)] \tag{1}$$

The absolute value of the minor principal stress σ_2 at failure as a function of α is the compressive stress:

$$\sigma_2 = \frac{q_{mc}}{\pi}\cdot[\alpha - \sin(\alpha)] \tag{2}$$

The limit stresses to which a brittle material can be subjected may be described by a two-dimensional failure envelope, which is defined to be the curve that circumscribes every single ultimate Mohr's circles. A failure envelope is hence the locus of the points that consist of ultimate combinations of σ and τ on any infinitesimal plane through any point in the material. The two coordinates σ and τ of a point of the curve define a stress vector that, if acting at any point of the material (having any direction), will trigger the failure of the material at this point and at any plane through this point that transmits the stresses σ and τ. Conversely, two coordinates σ and τ within the failure envelope will not cause the material to fail, whatever the plane.

The intersection of the failure envelope with the ordinate represents the shear strength without normal stress (cohesion) of that specific material. The intersection of the failure envelope with the abscissa represents the tensile strength of that specific material. In every masonry material, the latter is lower than the former. Consequently, a pure shear state causes masonry to fail by tensile rupture (axial breaking) due to the tensile principal stress (at 45°) and never by shear rupture (not by transverse sliding).

The two-dimensional failure criterion that best represents the experimental data on the collapse of masonry under a plane stress state is the Mohr-Coulomb criterion.

The Mohr-Coulomb failure criterion is a set of linear equations in principal stress space describing the conditions for which an isotropic material will fail, with any effect from the principal stress σ_3 being neglected. In this case, σ_3 (i.e., the out-of-plane principal stress) coincides with σ_z, which has been assumed to be zero.

The Mohr-Coulomb failure criterion is a contribution from Mohr and Coulomb, and the shape of the failure envelope (i.e., the loci of σ and τ acting on a failure plane) can be either a curve (Mohr's failure envelope) or, as a simplifying alternative, a straight line (Coulomb's failure envelop).

Since failure is dictated by the two-dimensional compressive stress state described by Eqs. (1) and (2), the Mohr's circle that dictates the failure lies entirely in the compression quadrants of the Mohr coordinate system (2nd and 3rd quadrants). Failure occurs for the σ_1 and σ_2 that are represented by a Mohr's circle which is tangent to the failure envelope, while the Mohr's circles of all the other points of the masonry do not touch the failure envelope. In other words, failure occurs when, in a point of the masonry surrounding the anchor, the difference between the major principal stress σ_1 minus the minor principal stress σ_2, which is the diameter of the Mohr's circle, causes that circle to be tangent to the failure envelope, while in all the other points of the masonry the diameters of the Mohr's circles are lower (Fig. 17).

A stress state whose Mohr's circle is tangent to the failure envelope corresponds to the failure. That is a stress failure, not a strain failure. Accordingly, on the plane that corresponds to the tangency, on one hand, a greater σ (or τ) with the same τ (or σ) is impossible. On the other hand, however, those stresses do not necessarily cause the material to break. The possible rupture depends on the plasticity that the material can display. In this case the plasticity is infinite, so no rupture can occur in the masonry.

The tangency corresponds thus to a local stress failure, while the anchor's failure occurs only when that stress state is reached by all the masonry involved in the kinematic mechanism, i.e., when the anchor is subjected to the two strip loads. The curve defined by the α-coordinate together with the two strip loads imply that the shear strength of the anchor is reached when the tangency to the failure envelope is reached not only at one point in the masonry, but at a three-dimensional masonry surface. In fact, the points of that α-curve have the same stress, which is the same for any z-coordinate. Ultimately, anchor's failure triggers not at a point, but at a pseudo-cylindrical surface whose height is $L - e$. For the sake of completeness, given that the strip loads are two with different directions, the pseudo-cylinders are two, one with positive y and the other one with negative y.

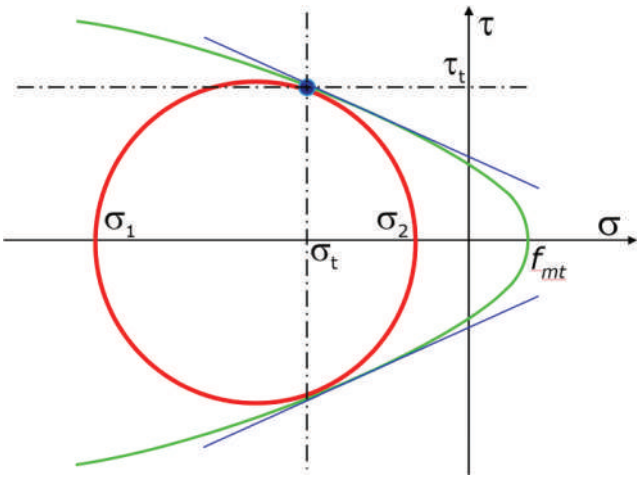

Fig. 17. Mohr's plane σ-τ (compressive stress is on the left of the σ-axis), Mohr failure envelope, masonry tensile strength f_{mt}, and Mohr's circles that dictates the shear strength of the anchor. The circle corresponds to the point stress state that triggers the failure of the masonry surrounding the anchor, whose principal stresses are σ_1 and σ_2 and whose diameter is $\sigma_1 - \sigma_2$. The figure also shows the tangency point of the Mohr's circle to the failure envelope (thick point), whose coordinates are σ_t and τ_t. Failure triggers at the point in the masonry with that stress state and at the plane that corresponds to that point. The two straight lines tangent to the Mohr failure envelope represent the Coulomb failure envelope defined by Eq. (5).

The tangency of the Mohr's circle to the failure envelope can be expressed using the normal and shear stresses, in lieu of the principal stresses. Accordingly, the infinitesimal plane through the point where failure occurs is subjected to the σ and τ stresses defined by the tangent point (the abscissa and the ordinate, respectively). Conversely, the σ and τ on all the other planes through that point and on the planes through all the other points are inside the failure envelope (Fig. 17).

The diameter d_m of the Mohr's circles that dictates the failure is expressed by the following function of α (Fig. 17):

$$d_m = \frac{2}{\pi}\cdot q_{mc}\cdot\sin(\alpha) \equiv 0.637\cdot q_{mc}\cdot\sin(\alpha) \tag{3}$$

The structural demand posed by the strip load to the masonry is represented by the diameter d_m together with the center of the relevant Mohr's circle, σ_a:

$$\sigma_a = \frac{\sigma_1 + \sigma_3}{2} \tag{4}$$

Clearly, σ_a is the average stress of the two principal stresses (Fig. 17).

The slope of the tangents to the Mohr's failure envelope decreases as the absolute value of the normal stress of that point increases, while the tangents of the Coulomb's failure envelope have all the same slope (Fig. 17). The slope represents the friction coefficient of that specific masonry for a given point of the curve. Masonry friction coefficient is denoted by μ. It is to note that μ is the trigonometric tangent of the masonry friction angle φ, i.e., $\mu = \tan(\varphi)$, whereas this paper refers to μ and not to φ.

Since μ for a Mohr's circle tangent to the failure envelope depends on the position of that circle in the Mohr's coordinate, in the end μ depends on σ_a, i.e., $\mu(\sigma_a)$.

The Mohr-Coulomb criterion is hence defined by a material constant, i.e., f_m, and either a material function, i.e., $\mu(\sigma_a)$, if the Mohr's failure envelope is referred to, or a material constant, i.e., μ, if the Coulomb's failure envelope is referred to. Those parameters must be defined in advance in order to have available the failure envelope.

The masonry crushing strength f_m is a principal stress, so the relevant point lies on the abscissa of the Mohr coordinate system (i.e., the absolute value of the abscissa of that point is f_m and the ordinate is zero). Accordingly, the Mohr's circle for uniaxial compressive strength is tangent to the ordinate ($\sigma_2 = 0$).

The value of f_m either can be measured on site by the double flat-jack test or can be borrowed from codes and literature for the specific masonry that the anchor is (or will be) embedded into.

The friction coefficient μ can be obtained from on-site tests or can be borrowed from codes and literature as well. The on-site tests that allow μ to be measured are the direct shear test and the shove test. Referring to the function $\mu(\sigma_a)$, i.e., using the Mohr's condition, the masonry must be subjected to different values of σ and the ultimate shear force must be measured for each σ. Referring to the material constant μ, i.e., using the Coulomb's condition, the masonry can be subjected to only one σ. In both the cases, the normal stress σ can be generated using the double flat-jack technique.

The theoretical analysis led to a result that allows the simple Coulomb's condition to be applied as if it were the more sophisticated Mohr's condition. It was proven, as shown in Fig. 17, that the Coulomb's failure envelope can accurately describe the failure of the anchor as long

as the friction coefficient μ is that for $\sigma = 0.33 \cdot \sigma_a$. The function $\mu(\sigma_a)$ can hence be replaced by:

$$\mu = \mu(0.33 \cdot \sigma_a) \tag{5}$$

The average stress σ_a can be expressed as a function of q_{mc}. That function can be obtained replacing σ_1 and σ_2 of (4) with Eqs. (1) and (2):

$$\sigma_a = \frac{q_{mc}}{\pi} \cdot \alpha \tag{6}$$

In (5), σ_a can be replaced by (6):

$$\mu = \mu\left(0.33 \cdot \frac{q_{mc}}{\pi} \cdot \alpha\right) \tag{7}$$

The terms into parenthesis of (5) and (7) are the normal stress to apply to the masonry by the double flat jacks in correspondence of which the ultimate shear force has to be measured.

Conversely to the function $\mu(\sigma_a)$, the expression (7) requires only one value of the normal stress. However, when (7) is used, q_{mc} is not yet known. In fact, Eq. (7) is devoted to calculating q_{mc}, but it contains q_{mc}. Thus, (7) must be used iteratively. However, the dependency of μ on σ is weak. Thus, the value of q_{mc} to plug into Eq. (7) has not to be necessary very close to the actual value. The direct shear test or the shove test performed for two different σ stresses is often enough. Only rarely it is necessary to perform the test for three or more σ, whereas more than sometimes one σ is enough.

Ultimately, expression (7) in lieu of $\mu(\sigma_a)$ simplifies on-site testing of masonry or literature research with no more than a marginal decrease in accuracy.

Sensitivity analysis determined that the friction coefficient μ weakly affects the shear strength of the anchor V_u. That outcome, together with the weak dependency of μ on σ, led to a more simplistic result, which allows the failure condition to be applied very easily, although with less accuracy than (7). In fact, it was proven that, for brickwork or stonework with lime mortar, $\mu = 0.45$ is simultaneously safe and realistic, although less precise. If $\mu = 0.45$ is used, no tests and no reference to literature are necessary.

Eventually, using the Coulomb's condition, the failure criterion is defined by two material constants – namely, 1- the one-dimensional stress that causes the masonry to fail f_m, 2- the internal friction coefficient μ, where μ is independent of σ. The Coulomb's condition can be applied in three ways – namely, using a generic σ, or the function value (7), or else $\mu = 0.45$.

In brief, the failure condition can be applied by choosing among the four different options given above. This is tantamount to say that μ can be obtained from choosing among four different methods, the more accurate the more demanding to obtain. The first option, which is the most accurate, is to apply the Mohr's condition, which entail the use of $\mu(\sigma_a)$. The second option, which is a little bit less accurate, is to apply the expression (7), which may require some iterations. The third option is to apply the Coulomb's condition for only a value of σ (i.e., not iteratively), whose accuracy depend on the distance between that σ and the real σ. The fourth option, which is the least accurate although its accuracy is more often than sometimes sufficient, is to apply the Coulomb's condition using $\mu = 0.45$. While the fourth option does not require any on-site measure or any archival research, the first, second, and third options require measuring μ on site, or alternatively searching and extracting that information from literature. On-site testing activity required by the first option is more demanding than that required by the second option, which in turn can be a little bit more demanding that that required by the third option.

The experiments of Sections 2 and 3 have referred to the second option, i.e., expression (7). The adequate value of the normal stress to induce in the masonry subjected to the shear test was ever found with no more than two iterations. Nonetheless, this model can be applied using whatever of the four options.

The theoretical analysis demonstrated that the strip load triggers local masonry failure when the diameter d_m reaches the following value (<Fig. 17):

$$d_m = f_m + 2 \cdot \mu \cdot \left(\sigma_a - \frac{f_m}{2}\right) \tag{8}$$

in which d_m is defined by Eq. (3) and the center of the Mohr's circle (average stress) σ_a is defined by Eq. (4).

The stress at the point where failure occurs cannot be lower than f_m. Therefore:

$$\sigma_a \geq f_m/2 \tag{9}$$

Plugging Eqs. (3) and (6) into Eq. (8):

$$0.637 \cdot q_{mc} \cdot \sin(\alpha) = f_m + 2 \cdot \mu \cdot \left(\frac{q_{mc}}{\pi} \cdot \alpha - \frac{f_m}{2}\right) \tag{10}$$

Eq. (10) can be solved for q_{mc}:

$$q_{mc} = \frac{\pi \cdot f_m \cdot (1 - \mu)}{2 \cdot [\sin(\alpha) - \mu \cdot \alpha]} \equiv \frac{1.571 \cdot f_m \cdot (1 - \mu)}{\sin(\alpha) - \mu \cdot \alpha} \tag{11}$$

Eq. (11) is a function of α. As such, it yields the value of q_{mc} that causes failure to occur at a certain α. The real value of q_{mc} is the minimum of all the values furnished by Eq. (11) for the α-values that satisfy Eq. (9). Accordingly, (11) is a function whose domain is the set of α-values that imply σ_a greater than or equal to $f_m / 2$ (i.e., inequation 9), and whose codomain is a set of q_{mc}-values which are the level of the strip loading that triggers masonry failure of the points whose angular coordinate is α. The minimum value of the codomain is the actual value of q_{mc}.

Eq. (9) can be rewritten using Eq. (7):

$$\frac{q_{mc}}{\pi} \cdot \alpha \geqslant \frac{f_m}{2} \tag{12}$$

Eq. (12) can be rearranged so as to isolate q_{mc}:

$$q_{mc} > \frac{\pi}{2 \cdot \alpha} \cdot f_m \equiv \frac{1.571}{\alpha} \cdot f_m \tag{13}$$

Eventually, q_{mc} is the minimum of (11) that respects the inequality (13).

The codomain (i.e., the values of q_{mc}) approaches positive infinity at the beginning and at the end of the domain of α. So, the minimum occurs for a value of α in the middle of the domain (i.e., its tangent is zero).

For the sake of depicting the complete picture, the α-values that are outside the domain cause the denominator of (11) to be negative or zero. If those values of α are plugged into (11), therefore, the values of q_{mc} that result are negative and approach negative infinity. Negative values of q_{mc} are however inadmissible, so those solutions have to be discarded.

Ultimately, the ultimate contact pressures consist of two strip loads of magnitude q_{mc} defined by Eqs. (11) and (13), acting with different direction on the right and on the left of the rotation center, respectively, apart from the two segments *a* and *d*.

An example of application of the formulas that provide the bi-axial compressive strength of the masonry, i.e., q_{mc}, is shown in Fig. 18.

5.2. Crushing strength and internal friction angle to use in the model

It has been shown that the ultimate limit state consists in a stress failure and that the stresses reach the strength of the masonry (ultimate value) on a double pseudo-cylinder (one pseudo-cylinder is the inverse of the other one).

Upon this a question arises: what component dictates f_m, the whole masonry assembly or the individual block, being the latter typically stronger than the former.

It has been proven that whatever the angle α that results from Eqs. (11) and (13), the maximum distance between the locus of the failure

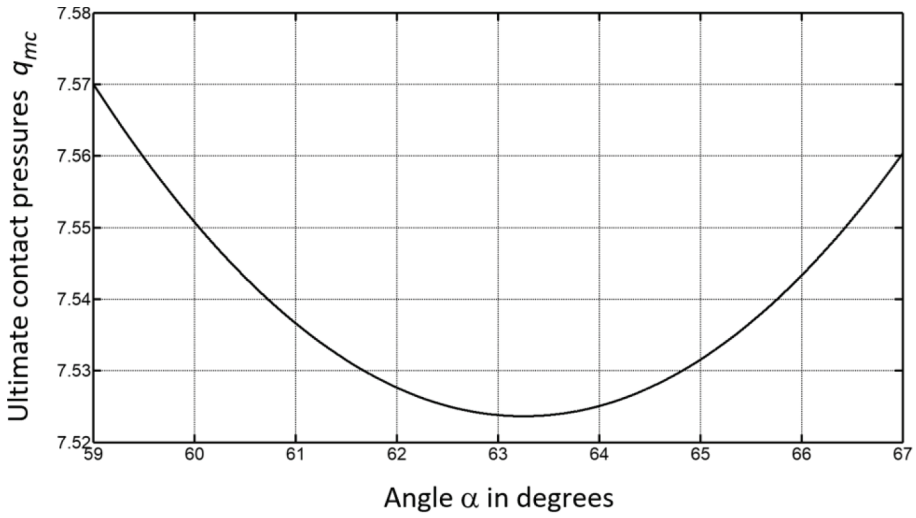

Fig. 18. Graphic of Eq. (11) within the limit of Eq. (13), for the masonry with $f_m = 3.45$ N/mm^2 and μ = 0.45, which is the fourth case of Table 2 presented in Subsection 6.1. Abscissa: coordinate α, in degrees. Ordinate: value of the ultimate contact pressures q_{mc}, in N/mm^2. As shown by the figure, the minimum value is $q_{mc} = 7.524$ N/mm^2 and it occurs at α = 63.3° ≡ 1.105 rad. The former defines the value of the ultimate contact pressures that dictate the failure, while the latter identifies the points within the masonry that dictate the failure of the anchor (stress failure).

points and the surface of the drilled hole occurs where the pseudo-cylinder intersects the *y*-axis. That distance, which is denoted by δ, is hence equal to:

$$\delta = \frac{\phi}{2 \cdot \tan\left(\frac{\alpha_u}{2}\right)} \tag{14}$$

where α_u is the α-coordinate of the failure points. The distance δ is thus the *y*-coordinate of the failure point that lies on the axis *y* minus ϕ/2, given that it is the point closest to the ancor.

However, the reliability of a shear strength dictated by the block depends on whether the block can actually reach its full strength. As observed in Subsection 1.4, only a specific model can predict if the shear strength of the anchor is dictated by the masonry strength or the block strength. The Reader who will use this model can choose whether to use the former or the latter. The case studies of Section 6 have used masonry strength. So, the values of Table 2 (presented in Subsection 6.1) are safe (in addition, those case studies assume that block surface failure will occur, which increases the conservativeness).

In any case, that choice must be supported by the knowledge of the loci of the points that dictate failure, i.e., the pseudo-cylinders. That knowledge can be condensed into the value of δ furnished by (14). If δ turns out to be greater than or only slighter lower than the distance of the anchor from the edge of the block it is embedded into, f_m must be the crushing strength of masonry. If conversely δ turns out to be substantially lower than the distance of the anchor from the edge of the block, the choice depends on the degree of flatness of the minimum of Eq. (11), i.e., on the second derivative of Eq. (11). In terms of fact, q_{mc} shall be the minimum between the value obtained using the strength of the block and the value obtained using the strength of the masonry together with an α close to the edge of the block.

5.3. Block surface failure

Contrary to the stress state at ultimate, the strain state is obviously not constant along the depth of the wall but varies along the *z*-axis according to the displacements of the anchor (Figs. 1 and 19). Therefore, the strains reach the maximum at the masonry surface.

Table 2
Case studies: purposely selected anchors and masonry types. The table exhibits the shear strength of 15 anchors embedded into brickwork and stonework. The 1st column specifies the type of masonry (only for the sake of completeness, given that this piece of information plays no role): bl = brickwork with lime mortar; bc = brickwork with cement mortar; sl = stonework with lime mortar. The columns from the 2nd to 6th provide the data of the model: Mechanical characteristics of the masonry (2nd and 3rd columns) and geometrical characteristics of the anchorage (4th, 5th, and 6th columns). The columns from the 7th to 11th report the results provided by the model: Ultimate contact pressures and depth of the failure point (7th and 8th columns, respectively); shear strength of the anchor calculated using the rigorous model, V_u, i.e., with Eqs. (17) and (18), together with the model of Section 5.1, which is in the 4th to last column; upper bound of the shear strength $V_{u\text{-max}}$, i.e., the value calculated using Eq. (20), which is in the 3rd to last column; and shear strength obtained with the simplified formula, $V_{u\text{-}sim}$, i.e., Eq. (21), which is reported in the 2nd to last column. The last column reports the elastic limit value of the shear strength, V_e.

	Data of the models					Results from the models					
	f_m	μ	ϕ	L	e	q_{mc}	δ	V_u	$V_{u\text{-max}}$	$V_{u\text{-}sim}$	V_e
	N/mm^2	/	mm	mm	mm	N/mm^2	mm	kN	kN	kN	kN
bl	2.60	0.40	17.5	265.0	15.0	5.41	13.0	6.505	10.387	8.017	5.429
bl	2.60	0.40	17.5	365.0	15.0	5.41	13.0	10.331	14.306	11.657	7.784
bl	7.40	0.65	26.0	330.0	30.0	20.46	28.5	37.933	72.676	52.497	34.693
bl	3.45	0.45	13.0	210.0	10.0	7.52	10.6	5.593	8.499	6.719	4.547
bl	4.25	0.50	35.0	420.0	20.0	9.75	30.3	34.449	59.337	45.022	31.744
bl	5.35	0.33	23.0	350.0	25.0	10.49	16.1	20.991	34.960	26.303	17.575
bc	8.15	0.55	20.5	295.0	35.0	19.76	18.9	25.080	49.472	35.404	21.907
bc	10.40	0.65	30.0	440.0	40.0	28.76	33.3	87.646	157.168	116.147	75.026
sl	1.00	0.35	16.5	245.0	45.0	1.99	12.0	1.379	3.331	2.162	1.228
sl	2.10	0.40	18.5	360.0	60.0	4.37	14.2	5.864	12.049	8.347	4.664
sl	6.30	0.45	21.0	195.0	55.0	13.74	40.6	4.481	23.294	11.620	6.354
sl	8.60	0.55	25.0	405.0	45.0	20.85	23.3	48.198	89.146	65.357	40.295
sl	1.50	0.33	12.5	148.0	8.0	2.94	8.6	1.273	2.252	1.665	1.185
sl	12.50	0.70	33.0	515.0	15.0	37.44	39.3	180.583	263.425	209.267	147.790
sl	1.80	0.30	10.0	103.0	3.0	3.45	6.9	0.829	1.471	1.087	0.825

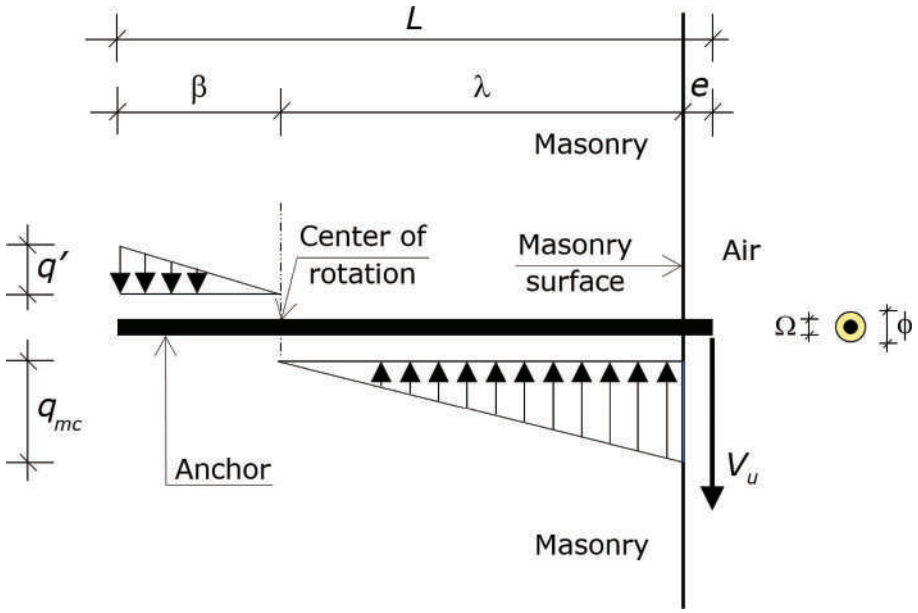

Fig. 19. Behavior of the anchor at the elastic limit. Contact pressures acting on the anchor, including the relevant symbols. The same pressures with opposite direction act on the boundary of the drilled hole. The cross-section shown on the right refers to the adhesive anchor. In the case of a mechanical anchor, $\Omega = \phi$.

The maximum strain is thus at the edge of the drilled hole and not far from a corner of a block, which gives rise to a singularity. As such, those points may not follow the Mohr-Coulomb criterion and their strength can be lower. Moreover, environmental actions could have caused a reduction in strength of an external layer of the block.

As a result, the anchor can cause a surface layer of the block to spall and detach from the masonry. Actually, the experimental results (Section 3) have proven that block surface failure occurs only in a minority of cases (not reported in this paper). In those cases, the layer that spalled had a thickness in proportion to the diameter of the drilled hole.

The experiments have also proven that block surface failure does not cause the anchorage to fail, but causes only the disappearance of the contact pressures transmitted by the layer that has spalled (layer delamination). The rest of the masonry continues transmitting the contact pressures. It follows that the anchorage can bear a shear force greater than that which has caused block surface failure. The model accounts for that behavior be virtue of Assumption 3 (Section 4).

Predictions of the shear force that causes block surface failure cannot be generalized because the event depends on many specific parameters, e.g., the radius of curvature of the drilled hole's edge and of the corners, the reduction in strength due to environmental actions, the thickness of the joints.

In respect to the above, the model that is presented allows the user to choose whether the masonry wall resists the contact pressures with the entire thickness or with the thickness minus a surface layer that is detached and, as such, plays no role in carrying the contact pressures. That choice can be made based on a specific local model, which has to predict not only whether block surface failure occurs or not, but also the thickness of the layer that detaches.

This model has made a simplifying and conservative assumption, which is that c is a fixed proportion to the diameter of the drilled hole ϕ and that this proportion is the one observed in the experimental campaigns:

$$c = 1.7 \cdot \phi \tag{15}$$

The applications of the model presented in this paper have assumed that block surface failure has occurred and have used c from (15). Nevertheless, the equations are written in a general form, which allows the user to choose whether to account for block surface failure or not, and, if yes, to choose the thickness of the layer that will be spalled. In fact, the equations include the thickness c of the detached layer, whose value can be zero or different than zero. In the latter case, who will use the model can either use Eq. (15) or derive c from a specific model [expression (10) of 22, 60–64].

It is essential to consider that block surface failure increases the lever arm of the shear force V, which in turn causes the bending moment in the anchor to increase. The check that the strength of the steel is sufficient to carry V_u must thus be accomplished using the lever arm $e + c$, i.e., if (15) is adopted: $e + 1.7 \cdot \phi$.

5.4. Model that predicts the shear strength of the anchor

This subsection presents the second step of the process. The contact pressures q_{mc} at failure consist of two uniform profiles, one directed upwards and the other directed downwards, which act onto the surrounding masonry and, with opposite direction, onto the embedded system (Fig. 2). The former are the compressive stresses that dictate the shear strength of the anchorage, while the latter are the stresses whose two resultants equilibrate the shear force applied at the anchor's external end.

The lengths of the two profiles of contact pressures q_{mc} depend on the position of the rotation center (Figs. 1 and 2). The problem that remains to solve has thus two unknowns: 1- the position of the center of rotation, whose distance is $\lambda + a + c + e$ from the external (free) end and $\beta + d$ from the internal (embedded) end; 2- and the shear strength of the anchor, V_u, which is the prediction the model aims at.

The position of the rotation center is obtained from the rotational equilibrium equation of the system. That equation is written with respect to the external end, so that the shear force is not included into the equation.

$$\phi \cdot \beta \cdot q_{mc} \cdot \left(\frac{\beta}{2} + d + a + \lambda + c + e \right) - \phi \cdot \lambda \cdot q_{mc} \cdot \left(\frac{\lambda}{2} + c + e \right) = 0 \tag{16}$$

Eq. (16) can be rewritten in the following form:

$$\beta \cdot \left(\frac{\beta}{2} + d + a + \lambda + c + e \right) - \lambda \cdot \left(\frac{\lambda}{2} + c + e \right) = 0 \tag{17}$$

Neither the diameter of the drilled hole nor the diameter of the anchor appears in Eq. (17). With regard to the diameter of the drilled hole, however, the model assumes that a, c, and d are in proportion to ϕ. Therefore, the position of the rotation center indirectly depends on the diameter of the drilled hole, although this dependence is weak. Not even the strength of masonry appears in Eq. (17), which implies that it does not influence the position of the rotation center.

Once the position of the rotation center has been identified, the shear strength V_u can be obtained from the (vertical) translational equilibrium of the system:

$$V_u = \phi\cdot\lambda\cdot q_{mc} - \phi\cdot\beta\cdot q_{mc} \equiv \phi\cdot q_{mc}\cdot(\lambda - \beta) \tag{18}$$

According to the comment about Eq. (17), λ and β depend on ϕ, which implies that Eq. (18) is not linear with respect to ϕ. Everything else being equal, hence, the shear strength is not in proportion to the diameter of the drilled hole.

The geometric parameters satisfy the relationship: $\beta + d + \lambda + a + c + e = L$ (Fig. 2). In that expression, β and λ are unknown, while the other parameters belong to the data. Thus, β can be expressed as a function of λ or vice versa. Ergo, Eq. (17) includes only one unknown, which is derived solving the equation. In so doing, the position of the rotation center is obtained, and in cascade β and λ are obtained as well.

Those values of β and λ are then plugged into Eq. (18). In so doing, the shear strength V_u of the anchor embedded into masonry is obtained, which solves the problem.

The equations are expressed in closed form. Consequently, the model provides two explicit formulas. Nevertheless, the substitution of β as a function of λ or vice versa, and the resulting explicit formula that gives λ or β is both cumbersome and useless. The Reader who will use this model shall find easier to solve the equation using a mathematical program, which is what the present writer has done for the case studies presented here. Therefore, the explicit formulas are not presented.

The model requires putting the values of c, a, and d into Eqs. (17) and (18). The applications of the model presented in this paper have assumed $c = 1.7\cdot\phi$, $a = \phi$, and $d = \phi$. That value of c has been justified in Subsection 5.3. The values of a and d were obtained analytically elaborating the experimental results. As previously mentioned, the Reader who will use this model can either adopt those values or determine the parameters c, a, and d using other criteria and formulas.

Eventually, the final form of the model is expressed by Eqs. (17) and (18). The model requires knowing only the compressive strength and friction angle of the masonry, as well as the geometry of the anchor.

The solution of Eq. (17) at $c = a = d = e = 0$ is representative, since it is the upper bound of the shear strength for an anchor of given drilled hole ϕ and given length L, embedded into a given masonry.

The shear strength obtained in this fashion is denoted by $V_{u\text{-max}}$, given that it is the upper bound (pedex "max") of the ultimate shear force (pedex "u").

Plugging those values of the parameters c, a, d, and e, Eq. (17) turns into:

$$\beta\cdot\left(\frac{\beta}{2} + \lambda\right) - \frac{\lambda^2}{2} = 0 \tag{19}$$

Those values of the parameters also imply that $\lambda = L - \beta$. Replacing λ with $L - \beta$ into Eq. (19), the second order equation that shows up can be solved in an expressive way, which is therefore presented. For the sake of completeness, it should be observed that only one of the two solutions lies inside the length L. So, the other solution has to be discarded.

The valid solution of Eq. (19) is: $\beta = 0.293\cdot L$. It follows that $\lambda = 0.707\cdot L$. Plugging those values into Eq. (18) the shear strength $V_{u\text{-max}}$ results to be:

$$V_{u-max} = 0.414\cdot\phi\cdot L\cdot q_{mc} \tag{20}$$

Ultimately, Eq. (20) is the upper bound of the shear strength of an anchor inserted into a drilled hole of diameter ϕ and embedded for the length L into a masonry that implies contact stresses equal to q_{mc}, where this value is given by Eqs. (11) and (13).

5.5. Simplified formula

Activity was then directed at searching for a simplified version of the model constituted of a single, quick formula. To that end, some terms of Eqs. (17) and (18) were approximated by simpler ones. In so doing the following formula was obtained, in which the simplified shear strength is denoted by $V_{u\text{-}sim}$.

$$V_{u-sim} = \frac{0.80\cdot(L - e - 1.7\cdot\phi)\cdot\phi\cdot f_m}{1.4 - \mu} \tag{21}$$

The simplified nature of Eq. (21) has suggested including the effect of block surface failure into the formula, and to use Eq. (15) to describe this event.

A wide-ranging analysis, which included not only the case studies presented in the paper but also supplementary customary cases and less typical or atypical cases, demonstrated that (21) gives a first, although rough, approximation of the anchor's shear strength.

Eq. (21) in lieu of the rigorous model permits the designer, not only to replace Eqs. (17) and (18) with a quicker formula, but also to spare computing q_{mc}. It can be anticipated from Section 7 that accuracy of (21) is adequate for preliminary dimensioning. All things considered Eq. (21) is a tool suitable for defining the geometry of the anchorage at the initial design stage. Then, once the geometry has been defined, the anchorage should be subjected to structural verification using the rigorous model.

5.6. Elastic shear strength of the anchor

The research work constructed the elastic model as well, since the elastic limit shear strength, which is denoted by V_e, plays a certain role in defining the safety factor (Fig. 15 shows both V_u and V_e).

Given that the rigid body model is adequate for describing the ultimate displacements, it is also adequate for describing the elastic displacements. Thus, Fig. 1 also represents the displacements of the anchor at the elastic limit. It follows that the strains at the drilled hole have a straight profile, which is zero at the rotation center (the elastic rotation center is obviously different than the ultimate rotation center). The profile of the contact pressures at the elastic limit derives directly from that strain profile (Fig. 19).

The elastic model is based on that assumption (i.e., Assumption 1), together with Assumptions 2, and 4 of the ultimate limit state (Section 4), while Assumption 3 plays no role in the elastic behavior, as the elastic behavior prevents block surface failure from occurring.

Assumption 4 entails that the elastic limit of the contact pressures is q_{mc}. At the elastic limit, hence, the contact pressures reach the same value reached at the ultimate, but in the former case the two distributions are triangular (Fig. 19), while in the latter case are uniform (Fig. 2).

The contact pressures at the elastic limit allow the rotational and translational equilibria to be written.

The rotational equilibrium equation is written again with respect to the external end (Fig. 19).

$$\phi\cdot\frac{\beta}{2}\cdot q'\cdot\left(\frac{2\cdot\beta}{3} + \lambda + e\right) - \phi\cdot\frac{\lambda}{2}\cdot q_{mc}\cdot\left(\frac{\lambda}{3} + e\right) = 0 \tag{22}$$

where q' is the contact pressure at the internal end, which is in proportion to q_{mc} (Fig. 19). Since $\beta < \lambda$, it follows that $q' < q_{mc}$. Precisely, $q' = \beta\cdot q_{mc}/\lambda$, which allows for eliminating q' from Eq. (22).

$$\phi\cdot\frac{\beta^2}{2}\cdot\frac{q_{mc}}{\lambda}\cdot\left(\frac{2\cdot\beta}{3} + \lambda + e\right) - \phi\cdot\frac{\lambda}{2}\cdot q_{mc}\cdot\left(\frac{\lambda}{3} + e\right) = 0 \tag{23}$$

Eq. (23) can then be rewritten in the following form:

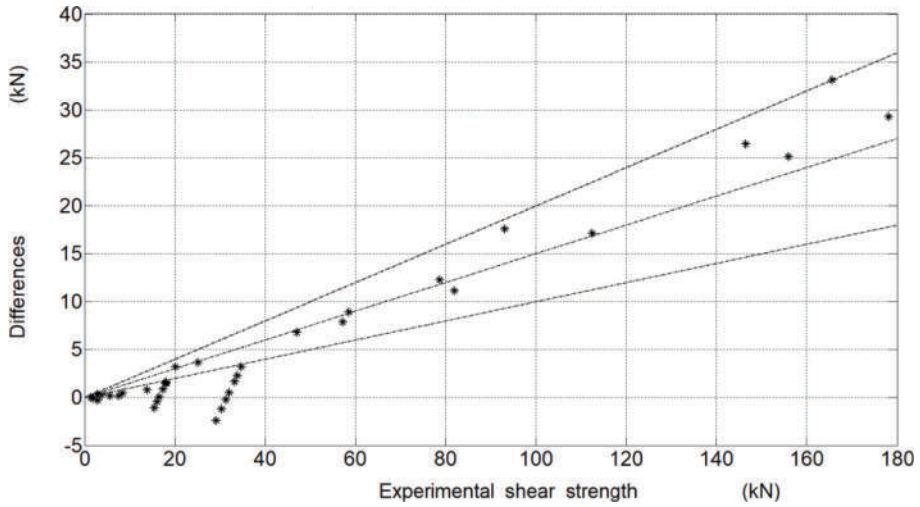

Fig. 20. Each asterisk represents an experiment of Tab 1. (Sections 2 and 3). Abscissa: experimental shear strength. Ordinate: experimental minus predicted shear strength (deviation). The lowest dash-dot straight line indicates the positive relative deviations of 10 %, the intermediate indicates the relative deviation of 15 %, and the top of 20 %.

$$\frac{\beta^2}{\lambda}\cdot\left(\frac{2\cdot\beta}{3}+\lambda+e\right)-\lambda\cdot\left(\frac{\lambda}{3}+e\right)=0 \tag{24}$$

The translational equilibrium equation in the direction of the shear force gives:

$$V_e=\frac{\phi\cdot\lambda\cdot q_{mc}}{2}-\frac{\phi\cdot\beta^2\cdot q_{mc}}{2\cdot\lambda}\equiv\phi\cdot q_{mc}\cdot\frac{\left(\lambda-\frac{\beta^2}{\lambda}\right)}{2} \tag{25}$$

The geometric parameters satisfy the relationship: $\beta+\lambda+e=L$ (Fig. 19). Given that e belongs to the data, β can be expressed as a function of λ, or vice versa. Thus, Eq. (24) includes only one unknown, which can be derived solving the equation. In so doing, λ is determined, and in cascade β too (or vice versa). Then, putting those values of β and λ into Eq. (25), the elastic shear strength V_e is obtained.

Again, the substitution of β as a function of λ (or vice versa) and the resulting explicit formula that gives λ (or β) is not presented here, since it is easier to solve the equation using a mathematical program.

6. Experimental verification, case studies, and code provisions

Every experiment was simulated by the model presented in Section 5. None of the experiments reported here exhibited the block surface failure. Accordingly, the modeling of those cases set the parameter c equal to zero. The theoretical predictions are reported in Table 1, together with the experimental results. Table 1 allows hence for comparing the theoretical and experimental results. That comparison is also represented in Fig. 20.

Every deviation (difference between an experimental result minus the relevant theoretical prediction) is less than 20 % of the experimental result, while most of the deviations are no more than 15 %, and the deviations of the weakest anchors are less than 10 % of the relevant experimental result (Fig. 20).

The comparison confirms hence the capacity of the model to reproduce the ultimate limit state of an anchor embedded into masonry, which is the same as saying that the four mechanical assumptions accurately describe the ultimate behavior of the anchor. In fact, the model derives from those assumptions, which are the synthesis of the behavior observed in the experiments. By the transitivity property, the comparison between the experimental results from the tests and the theoretical results from the model measures not only the reliability of the model but also the accuracy of the assumptions.

Closer inspection of the results revealed that in the case of brickwork, almost all the deviations are less than 10 % of the relevant experimental result, which is the experimental error expected for the measures of the masonry compressive strength and friction angle. In the case of stonework, conversely, the deviations are more than 10 % of the relevant experimental result, which means that are beyond the expected experimental error. In the case of brickwork, furthermore, those differences are either positive or negative. In the case of stonework, conversely, all the differences are positive – namely, each experimental result is greater than the relevant theoretical prediction.

The reason for that lies in which strength parameters are used in the model. The predictions of Table 1 were obtained using the parameters of the stonework assembly (as well as those of the brickwork assembly), whereas in reality the contact pressures were resisted by the stone that the anchor was embedded into (Subsections 5.3). Indeed, replacing the compressive strength and friction angle of the stonework with those of the individual stone, the model provided theoretical predictions that differed no more than moderately from the relevant experimental result, and those differences were either positive or negative, as well as within the expected experimental error. That result, on one hand confirms again the predictive capacity of the model, but on the other hand suggests using the mechanical parameters of the stone in lieu of those of the stonework assembly, whereas the latter provides conservative predictions.

6.1. Practical applications of the model

This model was applied to a wide-ranging series of practical cases, in order to test the applicability of the formulation and to explore the ultimate behavior of shear anchors embedded into masonry. The analysis of those cases allowed a discussion to be developed and conclusions to be drawn (Sections 7 and 8).

Some of those case studies – data and results – are reported in Table 2. The case studies were selected referring to brickwork and stonework that are typically found in existing structures. The embedded length ($L-e$) and the diameter of the drilled hole ϕ were selected in proportion to the strength of the masonry.

For each case study, Table 2 exhibits the relevant free parameters of the model – namely, the crushing strength of masonry f_m (compressive strength against uniform one-dimensional stresses), the internal friction coefficient of masonry μ, the diameter of the drilled hole ϕ, the length of the anchor L, and the length that protrudes out of the masonry e.

Table 2 subdivides the case studies into brickwork with lime mortar, brickwork with cement mortar, and stonework with lime mortar. The

Table 3
Adhesive anchors embedded into brickwork extracted from Table 1. Each column compares the experimental and analytical results to the provisions from [22]. First row: ordinal number of Table 1. Second row: experimental results. Third row: theoretical predictions. Fourth row: provisions from the EOTA technical report [22].

		1st	2nd	3rd	4th	5th	6th	24th	25th	26th	27th	28th	29th
$V_{u\text{-}ex}$	kN	17.30	17.91	17.99	16.01	18.04	16.50	8.43	7.61	5.57	3.75	1.99	1.34
V_u	kN	16.464	16.464	16.464	16.464	16.464	16.464	7.981	7.436	5.409	3.470	2.115	1.362
$V_{u\text{-}a}$	kN	1.576	1.576	1.576	1.576	1.576	1.576	0.801	0.773	0.498	0.338	0.194	0.150

role played by the type of masonry in the shear strength is however entirely represented by f_m and μ. So, that subdivision directly plays no role and is presented only to justify the masonry mechanical parameters that have been adopted. Ergo, every result of Table 2 holds true whatever the masonry type whose values of f_m and μ are those of that case study.

Each case study of Table 2 has been analyzed in four different fashions. The first analysis has used the rigorous model, i.e., Eqs. (11), (13), (17), and (18), together with $c = 1.7{\cdot}\phi$, $a = \phi$, and $d = \phi$ and no contact pressures acting on a and d. In Table 2, the shear strength obtained in that fashion is denoted in the same way it has been denoted throughout the paper, i.e., V_u.

Table 2 also shows the maximum distance of the points that dictate the failure from the anchor's center. In many cases, the distance shows that failure occurs in masonry portions near the drilled hole. In the case of stonework, therefore, failure would be dictated by the individual block and not by the whole masonry, whereas the value of f_m and μ of Table 2 refer to the stonework.

The second analysis has used Eq. (20). As previously specified, that shear strength is the upper bound for the given masonry and anchor. In Table 2, the shear strength obtained in that fashion is denoted by $V_{u\text{-max}}$.

The third analysis has used Eq. (21), which is the shear strength from the simplified formula of Section 10. As previously specified, that shear strength is a first, rough approximation of V_u. In Table 2, the shear strength obtained in that fashion is denoted by $V_{u\text{-}sim}$.

The fourth analysis exhibited by Table 2 has used the elastic model presented in Subsection 5.6 and has calculated the elastic limit shear strength V_e.

The results of this research were also compared with the provisions from [22], which is one of the most important code documents. Comparison considered the adhesive anchors embedded into brickwork of Table 1, as that technical report is devoted only to this type of anchorages. The comparison, which are reported in Table 3, shows that the shear strength given by those formulas is excessively low. The reason is that the document does not consider the actual resisting mechanism, which is provided by the whole masonry, but the specific resisting mechanisms of brick and mortar, which individually are weak, while collectively are strong.

In brief, the existing equations from codes, instructions, and manufacturers' documents result in very low predictions of the anchor's shear strength, to the point that designs seem unreasonably conservative. Prompted by this, there were two major changes to anchor provisions in [65]. One change was to increase the shear capacity due to masonry crushing by 67 percent. The second change, which does not interest this paper, modified the interaction equation for combined tension and shear loading from a linear interaction to an elliptical interaction, increasing the calculated capacity of anchor bolts.

7. Discussion and proposed technical solution

The close agreement between the model predictions and the experimental results (Section 6; Table 1) is the direct consequence of how the model was constructed. Modeling process started with some experimental campaigns that allowed the anchor's ultimate behavior to be observed, comprehended, and interpreted. The experimental results were then translated into exhaustive mechanical assumptions that allowed an analytically model to be constructed.

It is hardly necessary to mention that the model was not calibrated against the experimental results, since it is a predictive model. As such, it is devoted to describing the behavior of any anchor, and not only of the anchors that were tested. Accordingly, the experiments were used to define the assumptions and not to tune some parameters. The comparison between the theoretical predictions and the experimental results is thus the measure of the descriptive ability of the assumptions and not the result of a calibration.

Every prediction furnished by the model is not only close to the relevant experimental value but even a little lower, which proves that the model is not only accurate but also fairly conservative. Conservativeness derives from having slightly overrated a and d, and from having ignored the elastic contact pressures along these two segments. The results of Table 2 include another significant conservative source; the occurrence of the block surface failure, i.e., the systematic application of $c = 1.7{\cdot}\phi$, whereas the tests showed that this failure mode occurs only seldom. However, the model can be applied using values of a, d, and c different than those used herein. For instance, the predictions of Table 1 have used $c = 0$ (no block surface failure), as the tests that they simulate did not exhibit block surface failure. Of course, the lower those values the greater the shear strength from the model.

All things considered, the application of the model using the values of a, d, and c as done herein provides the lower bound of the anchors' shear strength. Nonetheless, the real shear strength of an anchor is close to the lower bound. The predictions of the model are, hence, simultaneously safe and realistic.

Eq. (20) calculates the upper bound of the shear strength. But the upper bound is quite far from the lower bound (Table 2), and as such from the real shear strength. The proper use of Eq. (20) is thus to know the maximum shear strength that a given anchor installed into a given masonry can reach if the rotational capacity of the anchor is extremely high (the higher the rotation the lower a and d), if block surface failure does not occur ($c = 0$), and if e is small. In those cases, the upper bound is close to the lower bound.

Practically speaking, Eq. (20) should be used neither to execute safety verifications nor to design the anchor, but only to assist the designer in the initial choices that must be taken when the shear anchor is only one of several options in order to connect the attachment to the masonry wall. That is to say, (20) should only be used to decide whether the shear anchor is a viable solution to a certain problem.

Predictions of Eq. (21) are not far from the real values but are greater. So, they are not conservative. On one side, hence, (21) furnishes quite accurate, although unsafe, predictions. On the other side, however, (21) spares computing q_{mc} and consists of a single equation, while the model requires computing q_{mc} and consists of a two-equation system. The former is hence faster and easier than the latter. Al things considered, Eq. (21) is a viable tool at the design stage, but the capacity of the anchor must be assessed and verified using the analytical exact (rigorous) model.

Practically speaking, Eq. (21) should be used to define the length of the anchor, the diameters of drilled hole and anchor, the type of anchor and anchoring material, and the number of anchors in the case of anchor group. Then, the anchor that has been just designed must be verified using the rigorous model.

Sensitivity analysis has proven that the shear strength of the masonry anchor depends approximately proportionally on anchor length, drilled hole diameter, and masonry compressive strength. If one of those

parameters doubles and everything else remains the same, the shear strength of the anchor is also not so far from being double. Sensitivity analysis has also proven that the eccentricity greatly impacts the shear strength, and thus it must be kept as low as possible. Regarding masonry friction coefficient, sensitivity analysis has proven that on one hand, the greater it is, the greater is the anchor shear strength, but on the other hand, varying its value within a realistic range, the anchor shear strength varies no more than moderately, which allows for the simplification of the shear tests (Subsection 5.1).

The analytical model has revealed that the actual shear strength of an anchorage post-installed into masonry is dramatically higher than that obtainable from the formulations of codes and technical reports (Table 3). Those formulations underrate the real shear strength because they are empirical. In fact, each formula is the result of a calibration against experimental data obtained for given anchor's geometries embedded in given categories of masonry.

That approach ignores the real role played by anchor length, drilled hole diameter, and eccentricity. Moreover, masonry is suitable to be classified into categories only for the purpose of seismic analyses, but neither brickwork nor stonework is suitable to be classified into categories for the purpose of static analyses, let alone for predicting the shear strength of a masonry anchor.

Despite that, codes and technical reports calculate anchor's shear strength referring to classifications of masonry according to types of blocks and kind of mortar.

Brickwork is usually subdivided into three categories – namely, lime mortar, cement mortar, and hollow brick masonry (with cement mortar). That classification does not take into account the brick bond and the arrangement of the mortar joints, which conversely largely impact on the masonry compressive strength f_m and internal friction coefficient μ. Stonework (with lime mortar) is usually classified into 5–7 categories according to the type and arrangement of blocks (regular or irregular stone patterns, dressed or undressed stones, ashlar masonry or rubble masonry, etc.). Not even that classification is adequately representative because the compressive strength and internal friction coefficient vary substantially within each category. Ultimately, those classification are suitable for seismic analyses but not for static analyses, least of all for the masonry shear anchor.

For that reason, the experimental shear strengths measured for anchors having the same geometry and embedded into the same category of masonry exhibit extremely large dispersion, which makes the characteristic value be drastically lower than the average value. In other words, the 0.05-fractile of a statistical distribution of experimental shear strengths is dramatically lower that the 0.50-fractile. Ergo, the anchor's shear strength derived from experimental results obtained for a certain category of masonry are excessively small.

Those values respect only the statistics, while they do not consider at all the mechanical behavior of the anchor, i.e., they result from a black-box model. On the contrary, the model presented in this paper simulates the actual mechanical behavior of the anchor, and therefore it does not suffer from the disadvantage of the black-box approach (i.e., it is a predictive analytical model). For that reason, this model provides anchors' shear strengths that simultaneously are truly realistic, substantially greater, and systematically safe.

The points at which the greatest circle of Mohr touch the failure envelope curve are often close to the anchor (δ in Table 2), which allows the designer to make some evaluations about the values of the masonry crushing strength f_m and internal friction angle μ to use in the model. Especially for the stonework, the distance δ often implies that the points that dictate q_{mc} are not only within the block but also far from its edges, which is a favorable condition. In that case the designer can either neglect this condition, which leads to a totally conservative position, or consider it, which implies a less conservative position but a greater strength. In the former case, q_{mc} is calculated using f_m and μ of the whole masonry. In the latter case, q_{mc} is calculated using f_m and μ of the individual block, which are greater. In the latter case, however, the designer must also calculate q_{mc} using the α of the block's edge closest to the anchor, together with f_m and μ of the masonry. The value of q_{mc} to insert in the model must be the lowest one between them.

The direct comparison between the shear strength V_u and the elastic shear strength V_e made using the values presented in Table 2 is biased, since all those values account for block surface failure, which cannot occur during the elastic behavior. Accordingly, V_u of Table 2 is produced by the contact pressures q_{mc} acting along the length $(L - e - c - a - d)$, while V_e is produced by the contact pressures acting along the length $(L - e)$. Where the diameter ϕ of the drilled hole is large, and consequently c is large as well (in addition, a and d are large too), where the length L is short, and where the contact pressures q_{mc} are high, the resultant force of the contact pressures acting on the length c is appreciable (as well as those acting on a and d). Consequently, the segment c that is either considered or excluded in producing shear strength, as well as a and d, can make a great difference in the result, up to the point that the elastic shear strength V_e could even be greater than the ultimate shear strength V_u (this occurs for the 11th case of Table 2).

The comparison between the shear strength V_u and the elastic shear strength V_e should thus be made using V_u values obtained for $c = 0$ (no block surface failure). That comparison not only is consistent, but also is the litmus paper that reveals whether the design of the anchor is proper or not. If V_e turns out to be close to V_u, the post-failure behavior of the anchor is inadequate because the failure mode is too brittle. In that case, the anchor should be replaced by two smaller-diameter anchors (or more than two).

The maximum distance δ between the locus of the failure points and the anchor provides an estimation of how wide the portion of uncracked masonry around the anchor must be, so that the anchor be properly installed. It was proven that, if a strip of length equal to or greater than 5·δ and width at least equal to 2·ϕ is uncracked, the compressive stress diffusion can occur adequately. In all the case studies, δ was found in the range 7–44 mm. A strip of length 225 mm shall therefore be sufficient to almost any anchor.

The model – of course, in agreement with the experiments – has proven that anchor's shear strength depends on the diameter ϕ of the drilled hole; everything else being equal, the greater the diameter of the drilled hole the greater the shear strength of the anchor. However, the shear strength of the anchor is not in proportion to the diameter ϕ, for the reason explained about Eq. (17). Conversely, the shear strength was proven to be independent of the diameter Ω of the anchor, as long as the steel withstands the shear force that dictates masonry failure.

The analysis of a complete series of anchors (some of which are those of Table 2) has proven that in practical case steel rupture occurs for diameters Ω of the anchor substantially smaller than the diameter ϕ of the drilled hole. Accordingly, the model presented here shall be used to define ϕ and L, while Ω shall be defined so that simultaneously the anchor can bear V_u, the slenderness ratio L/Ω respects the limit of Subsection 3.1, and the gap complies with the conditions of Subsection 1.3.

That outcome prompted a technical modification of the traditional shear anchors, which consists of making ϕ and Ω be totally independent of one another, regardless the gap between anchor and drilled hole. The anchor that is proposed on the basis of this model is made of two components, whose insertion is dependent on a two-step process, after drilling the hole into the masonry (Fig. 21).

The first component is an internally threaded socket (manufactured from a steel pipe). That component is installed by means of the chemical-post installation process presented in Subsection 1.3, using a resin anchoring material. Accordingly, the diameter ϕ of the drilled hole must be greater than that of the socket of no more than 4.5–8.0 mm. Nevertheless, it can be installed using a mortar anchoring material (with a larger drilled hole), whereas the resin is usually a better technological solution for this application.

The second component is a screw or a threaded bar (or else a threaded rod). After the socket has been cured for the adequate number of days and temperature until it forms a chemical bond with the

Fig. 21. Technical solution conceived considering the results of the application of the model to practical cases. The two images show an anchor whose threaded socket has external diameters of 22 mm and whose screw has diameter of 14 mm. As shown by the image above, the anchor is composed of two components. As shown by the image below, the first component is an internally threaded socket, while the second one is a screw.

masonry, the screw (or the threaded bar/rod) is screwed into the threaded socket (Fig. 21).

With respect to the traditional solutions this solution facilitates post-installation because it guarantees no more than irrelevant deviations to the designed anchor position, and allows for large drilled holes not only with mortar anchoring materials but also with resin anchoring materials.

8. Conclusions

The research work, devoted to the post-installed horizontal anchor that transfers vertical loads from a horizontal structure that the loads act on to a vertical masonry structure, was composed of a comprehensive experimental work followed by a theoretical study based on the experimental results. The research has given birth to this paper, which has presented an analytical, closed-form model that simulates the ultimate behavior of the anchorage subjected to shear force.

The model presented in this paper allows the structural designer to predict the shear strength of an anchor embedded into masonry. In order to utilize the model, the data that must be known is comprised of: the crushing (compressive) strength and friction angle of the masonry, the diameter and length of the anchor, and the length that protrudes from the masonry surface. Ergo, the model has five free parameters (i.e., five values that must be previously defined in order to use the model); two mechanical parameters, which are included into the basic information that must be available when an existing building is analyzed, and three geometric parameters, which are defined by the design of the anchor.

The model is based on four mechanical assumptions. The predictive capacity of the model and its reliability coincide hence with the representativeness of those underlying assumptions. The modeling assumptions were derived from experimental campaigns executed on anchors post-installed into real masonry structures of historical buildings (not in laboratory). Both adhesive and mechanical anchors were tested. In the cases of adhesive anchors, both resin and mortar were used. The assumptions are the synthesis of the experimental observations. Needless to say, the model simulates the experiments with close agreement, as proven by the marginal differences between the theoretical predictions from the model and the experimental results from the tests.

This paper has also presented the model that predicts the elastic limit shear strength. The comparison between the elastic shear strength and the ultimate shear strength shall allow the designer to assess whether the failure mode is adequate, or the collapse is excessively brittle. That information shall also allow the editors of codes, standards, and regulations to define the most appropriate safety factors to apply to the theoretical predictions.

The application of the model has proven that the shear strengths obtained from the formulas provided by codes and technical reports are unreliable. The reason is that those formulas derive from mere statistic elaborations of experimental data obtained for specimens whose characteristics can be very different from each other. Consequently, the measures that are statistically elaborated exhibit a huge dispersion. Ultimately, an empirical approach does not suit to the shear anchor.

This model considers properly designed and installed anchors. Ergo, failure is dictated by the masonry that surrounds the drilled hole, and not by the anchor or the anchoring material. Moreover, the model considers anchors that use the entire potential capacity of the anchorage. Ergo, the anchor leaves adequate clearance from the boundaries, so that the boundary effect is negligible, and in the case of anchor groups the anchors leave adequate clearance from each other, so

that the group effect is negligible.

The model has proven that the greater the diameter of the drilled hole the greater the shear strength of the anchor, while the diameter of the anchor has no effects on the shear strength (as long as the anchor is not too slender or too thin). That result has suggested an improved technical solution; an anchor that is composed of a smaller diameter element enveloped by a larger diameter element, whose insertion is dependent on a two-phase process.

The next step of this research work will be the construction of a model to predict the shear strength of an anchor subjected to shear force and axial force simultaneously, and then a model to predict the shear strength of an anchor group embedded into masonry.

Declaration of Competing Interest

The author declares that he has no known competing financial interests or personal relationships that could have appeared to influence the work reported in this paper.

Data availability

No data was used for the research described in the article.

References

[1] Paganoni S, D'Ayala D. Testing and design procedure for corner connections of masonry heritage buildings strengthened by metallic grouted anchors. Eng Struct 2014;70(July):278–93.
[2] Fagone M, Rotunno T, Bertolesi E, Grande E, Milani G. experimental study on the local behavior of CFRP anchor spikes fixed to masonry substrates. Key Eng Mater 2022;916 KEM:361–8.
[3] ETAG 029. Guideline for European technical approval of metal injection anchors for use in masonry Edition April 2013.
[4] Bokor B, Sharma A, Hofmann J. Experimental investigations on the concrete edge failure of shear loaded anchor groups of rectangular and non-rectangular configurations. Eng Struct 2020;222:111153.
[5] Li X, Zhang J, Min X, Song S, Liu B, Yang Y, et al. Anchorage performance of group anchored 1860-grade high-strength steel strands for beam-column connection. Constr Build Mater 2022;349:128664.
[6] Stehle EJ, Sharma A. Concrete cone breakout behavior of anchor groups in uncracked concrete under displacement-controlled cyclic tension load. Eng Struct 2021;246:113092.
[7] Johnson TP, Dowell RK, Silva JF. A review of code seismic demands for anchorage of nonstructural components. Journal of Building Engineering 2016;5:249–53.
[8] Foraboschi P. Ultimate Shear Force of an Any Anchor Group Post-Installed into Concrete. Materials 2023;16(7).
[9] Moreira S, Ramos LF, Oliveira DV, Lourenço PB. Experimental behavior of masonry wall-to-timber elements connections strengthened with injection anchors. Eng Struct 2014;81(December):98–109.
[10] Corradi M, Borri A, Poverello E, Castori G. The use of transverse connectors as reinforcement of multi-leaf walls. Materials and Structures/Materiaux et Constructions 2017;50(2).
[11] Mirza O, Uy B. Effects of the combination of axial and shear loading on the behaviour of headed stud steel anchors. Eng Struct 2010;32(1):93–105.
[12] Llauradó Paula Villanueva, Ibell Tim, Gómez Jaime Fernández, González Ramos Francisco J. Pull-out and shear-strength models for FRP spike anchors. Compos B Eng 2017;116:239–52.
[13] Ceroni F, Darban H, Luciano R. Analysis of bond behavior of injected anchors in masonry elements by means of Finite Element Modeling. Compos Struct 2020;241 (June):112099.
[14] Piccinin R, Ballarini R, Cattaneo S. Pullout capacity of headed anchors in prestressed concrete. J Eng Mech 2012;138(7):877–87.
[15] Burton C, Visintin P, Griffith M, Vaculik J. Laboratory investigation of pull-out capacity of chemical anchors in individual new and vintage masonry units under quasi-static, cyclic and impact load. Structures 2021;34:901–30.
[16] Del Vecchio C, Maddaloni G. Maria Rosaria Pecce. Pull-out tests on injected steel anchors in a masonry tuff wallet. Procedia Struct Integrity 2023;44:1411–8.
[17] Dudek D, Kadela M. Pull-Out Strength of Resin Anchors in Non-cracked and Cracked Concrete and Masonry Substrates. Procedia Eng 2016;161:864–7.
[18] Noor Aina Misnon, Marta Giaretton, Jason Ingham, Dmytro Dizhur. Pull-out behaviour of near surface mounted steel wire rope bonded to clay-brick masonry. Structures 2021; 29: 199-210.
[19] Ceroni F, Darban H, Caterino N, Luciano R. Efficiency of injected anchors in masonry elements: Evaluation of pull-out strength. Constr Build Mater 2021;267: 121707.
[20] Specification for Masonry Structures, TMS 605-13/ACI 530.1-13/ASCE 6-13, Reported by the Masonry Standards Joint Committee, 2013.
[21] Standard Specification for Carbon Steel Bolts and Studs, 60,000 psi Tensile Strength, ASTM A307-12, ASTM International, 2012.
[22] European Organisation for Technical Assessment. Design methods for anchorages with metal injection anchors and screw anchors for use in masonry. Technical reports, TR 054, 2016, April.
[23] Standard Test Methods for Strength of Anchors in Concrete and Masonry Elements, ASTM E488-10, ASTM International, 2010.
[24] Cattaneo S. Wedge-type expansion anchors in high-performance concrete. ACI Struct J 2007;104(2):191–8.
[25] European Organisation for Technical Assessment. Recommendations for tests of metal injection anchors for use in masonry to be carried out on construction works. Technical reports, TR 053, 2016, April.
[26] Design of Anchor Bolts Embedded in Concrete Masonry, TEK 12-3A. National Concrete Masonry Association, 2004.
[27] Cattaneo S, Muciaccia G. Adhesive anchors in high performance concrete. Materials and Structures/Materiaux et Constructions 2016;49(7):2689–700.
[28] Braimah A, Guilbeault R, Contestabile E. Strain rate behaviour of adhesive anchors in masonry. Eng Struct 2014;67(May):96–108.
[29] Maione A, Casapulla C, Di Ludovico M, Prota A, Ceroni F. Efficiency of injected anchors in connecting T-shaped masonry walls: a modelling approach. Constr Build Mater 2021;301(September):124051.
[30] Ceroni F, Di Ludovico M. Traditional and innovative systems for injected anchors in masonry elements: Experimental behavior and theoretical formulations. Constr Build Mater 2020;254(September):119178.
[31] Ahmed LT, Braimah A. Shear behaviour of adhesive anchors under different strain rates. Eng Struct 2021;244:112763.
[32] Bertolesi E, Milani G, Grande E, Fagone M, Rotunno T. Numerical analysis of the bond behavior of FRP applied to masonry curved substrates with anchor spikes. Lecture Notes in Mechanical Engineering 2020:2149–61.
[33] Splices. Development and Standard Hooks for Concrete Masonry, TEK 12–6. National Concrete Masonry Association; 2007.
[34] Di Nunzio G, Pinoteau N, Muciaccia G, Guillet T, Mège R. Derivation of an innovative testing protocol for plastic anchors for fixing light façade claddings under seismic action. Eng Struct 2021;248:113191.
[35] Ivorra S, García-Barba J, Mateo M, Pérez-Carramiñana C, Maciá A. Partial collapse of a ventilated stone façade: Diagnosis and analysis of the anchorage system. Eng Fail Anal 2013;31:290–301.
[36] Ji Ru, Guo S, Wei S. Evaluation of anchor bolt effects on the thermal performance of building insulation materials. Journal of Building Engineering 2020;29:101200.
[37] Tubbs JB, Pollock DG, McLean DI. Testing of anchor bolts in concrete block masonry. The Masonry Society Journal 2000;18(2):75–88.
[38] Hou Y, Duan K, Cao S, Liu J, Jing D, Zhang Z. Experimental research on the behavior of masonry walls reinforced with dry-connected steel plate frames under axial compression. Journal of Building Engineering 2022;46(April):103732.
[39] International Building Code, International Code Council, 2012.
[40] International Residential Code, International Code Council, 2012.
[41] Standard Specification for Carbon Structural Steel, ASTM A36-12, ASTM International, 2012.
[42] Allowable Stress Design of Concrete Masonry, TEK 14-7C, National Concrete Masonry Association, 2011.
[43] Building Code Requirements for Masonry Structures, TMS 402-11/ACI 530-11/ ASCE 5-11, Reported by the Masonry Standards Joint Committee, 2011.
[44] Building Code Requirements for Masonry Structures, TMS 402-13/ACI 530-13/ ASCE 5-13, Reported by the Masonry Standards Joint Committee, 2013.
[45] Lee J-H, Cho B, Kim J-B, Lee K-J, Jung C-Y. Shear capacity of cast-in headed anchors in steel fiber-reinforced concrete. Eng Struct 2018;171:421–32.
[46] Vargas L, Sandoval C, Bertolesi E, Calderón S. Seismic behavior of partially grouted masonry shear walls containing openings: Experimental testing. Eng Struct 2023; 278:115549.
[47] F. Silveri, P. Riva, G. Profeta, A. Belleri, E. Poverello, P. Panzeri. San Giovanni Battista church: Operational modal analysis after injected anchors strengthening. Structural Analysis of Historical Constructions: Anamnesis, diagnosis, therapy, controls - Proceedings of the 10th International Conference on Structural Analysis of Historical Constructions, SAHC 2016, Leuven, 13-15 September 2016, Code 179659: 1125-1132.
[48] Silveri F, Riva P, Profeta G, Poverello E, Algeri C. Experimental Study on Injected Anchors for the Seismic Retrofit of Historical Masonry Buildings. International Journal of Architectural Heritage 2015;10(2–3):182–203.
[49] Olalusi OB, Spyridis P. Uncertainty modelling and analysis of the concrete edge breakout resistance of single anchors in shear. Eng Struct 2020;222:111112.
[50] Takase Y. Testing and modeling of dowel action for a post-installed anchor subjected to combined shear force and tensile force. Eng Struct 2019;195:551–8.
[51] Casolo S, Biolzi L, Carvelli V, Barbieri G. Testing masonry blockwork panels for orthotropic shear strength. Constr Build Mater 2019;214:74–92.
[52] Matsunaga K, Takase Y, Abe T. Modeling of dowel action for cast-in and post-installed anchors considering bond property. Eng Struct 2021;245:112773.
[53] Hain A, Zaghi AE. Experimental investigation of a simple shear connection to concrete-filled FRP tube (CFFT) columns. Eng Struct 2021;247:113174.
[54] Yavartanoo F, Kang T-K. Retrofitting of unreinforced masonry structures and considerations for heritage-sensitive constructions. Journal of Building. Engineering 2022;49(May):103993.
[55] Asjodi AH, Dolatshahi KM. Extended fragility surfaces for unreinforced masonry walls using vision-derived damage parameters. Eng Struct 2023;278:115467.
[56] Teschemacher T, Wilson P, Wüchner R, Bletzinger K-U. Macroscopic characterization of modern masonry. Eng Struct 2022;268:114630.

[57] Gregori A, Mercuri M, Angiolilli M, Pathirage M. Simulating defects in brick masonry panels subjected to compressive loads. Eng Struct 2022;263:114333.
[58] Guerreiro J, Gago AS, Ferreira J, Proença J. An innovative anchoring system for old masonry buildings. Journal of Building Engineering 2017;13(September):184–95.
[59] Dizhur D, Wei S, Giaretton M, Schultz AE, Ingham JM, Giongo I. Testing of URM wall-to-diaphragm through-bolt plate anchor connections. Earthq Spectra 2021;37 (1):304–23.
[60] Giuriani E, Gattesco N, Del Piccolo M. Experimental tests on the shear behaviour of dowels connecting concrete slabs to stone masonry walls. Mater Struct 1993;26(5): 293–301.
[61] Ramirez R, Muñoz R, Lourenço PB. On Mechanical Behavior of Metal Anchors in Historical Brick Masonry: Testing and Analytical Validation. Appl Sci 2023;13: 3999.
[62] Porcarelli S, Shedde D, Wang Z, Ingham JM, Giongo I, Dizhur D. Tension and shear anchorage systems for limestone structures. Constr Build Mater 2021;272:121616.
[63] I. Giongo, D. Dizhur, R. Tomasi, J. Ingham. In-situ testing of wall-to-diaphragm shear transferring connections in an existing clay brick URM building. 9th International Masonry Conference 2014 in Guimarães (Portugal).
[64] European Organisation for Technical Approvals). Design of Bonded Anchors (Technical Report TR 029); EOTA: Brussels, Belgium, 2010. Edition: June 2007. Amended September 2010.
[65] TMS 402. Building code Requirements for masonry structures. Revision of 2016 (formerly designated as ACI 530 and ASCE 5).
[66] TMS 602. Specifications for masonry structures. Revision of 2016 (formerly designated as ACI 530.1 and ASCE 6).
[67] M. J. Boussinesq. Application des potentiels a l'etude de l'equilibre et du mouvement des solides elastiques, principalement au calcul des deformations et des pressions que produisent, dans ces solides, des efforts quelconques exerces sur une petite partie de leur surface ou de leur interieur: Memoire suivi de notes etendues sur divers points de physique mathematique et d'analyse. GauthierVillars, 1885, Paris: pp. 722.
[68] S.D. Carothers. The Elastic Equivalence of Statically Equipollent Loads. Proceedings, International Mathematical Congress, Toronto, 1924-a; Vol. 11: 519-526.
[69] Carothers SD. Test Loads on Foundations as Affected by Scale of Tested Area. Proceedings, International Mathematical Congress, Toronto 1924;11:527–49.